8-10-2018

Urban Landscape Assessment of the Mississippi and Alabama Gulf Coast using Landsat Imagery 1973-2015

Abdalla R. Sherif

Urban landscape assessment of the Mississippi and Alabama Gulf Coast using Landsat imagery 1973-2015

By

Abdalla R. Sherif

A Thesis
Submitted to the Faculty of
Mississippi State University
in Partial Fulfillment of the Requirements
for the Degree of Master of Science
in Geospatial Sciences
in the Department of Geosciences

Mississippi State, Mississippi

August 2018

Urban landscape assessment of the Mississippi and Alabama Gulf Coast using Landsat imagery 1973-2015

By

Abdalla R. Sherif

Approved:

Qingmin Meng
(Major Professor)

Shrinidhi S. Ambinakudige
(Committee Member)

Nathaniel J. Gabriel
(Committee Member)

Renee M. Clary
(Graduate Coordinator)

Rick Travis
Dean
College of Arts & Sciences

Name: Abdalla R. Sherif

Date of Degree: August 10, 2018

Institution: Mississippi State University

Major Field: Geospatial Sciences

Committee: Qingmin Meng, Shrinidhi S. Ambinakudige, and Nathaniel J. Gabriel

Title of Study: Urban landscape assessment of the Mississippi and Alabama Gulf Coast using Landsat imagery 1973-2015

Pages in Study 67

Candidate for Degree of Master of Science

This study aims to conduct an assessment of the land cover change of the Mississippi and Alabama coastal region, an integral part of the Gulf Coast ecological makeup. Landsat satellite data were used to perform a supervised classification using the imagery captured by Landsat sensors including Landsat 1-2 Multispectral Scanner (MSS), Landsat 4-5 Thematic Mapper (TM), Landsat 7 Enhanced Thematic Mapper (ETM+), and Landsat 8 Operational Land Imager (OLI) from 1973 to 2015. The objective of this study is to build a long-term assessment of urban development and land cover change over the past four decades for the Alabama and Mississippi Gulf Coast and to characterize these changes using Landscape Metrics (LM). The findings of this study indicate that the urban land cover doubled in size between 1973 and 2015. This expansion was accompanied by a high degree of urban fragmentation during the first half of the study period and then a gradual leveling off. Local, state, and federal authorities can use the results of this study to build mitigation plans, coastal development planning, and serve as the primary evaluation of the current urban development for city planners,

environmental advocates, and community leaders to reduce degradation for this environmentally sensitive coastal region.

ACKNOWLEDGEMENTS

I would like to acknowledge my committee members for their guidance and contribution to my research throughout my time graduate degree program. I would like to thank the Department of Geosciences at Mississippi State University for providing me with the funding to complete my master's degree.

TABLE OF CONTENTS

LIST OF TABLES

LIST OF FIGURES

CHAPTER I

INTRODUCTION

1.1 Background

The Gulf Coast represents a valuable environmental and economic resource for the Southeastern region of the United States. It hosts a variety of major industries such as agriculture, forestry (Li and Meng, 2016), tourism (Ha, 2007), petroleum, petrochemical (Tipsword et al., 1966), seafood, shipping, and shipbuilding industries (Zhang et al., 2015). The variety of business districts and urban population centers within this region makes the coastal counties vital to the economies of Mississippi and Alabama (Crossett et al., 2004; Zhang et al., 2015). The Gulfport-Biloxi-Pascagoula Metropolitan area and the Mobile Metropolitan area are located in the study area (U.S. Census Bureau, 2011). This area experiences a higher urban development rate, and it has a 50% higher population growth than the rest of the region. Consequently, this growing population leads to an increasing development along coastal lines (Crossett et al., 2004). Increased environmental degradation and coastal pollution are directly linked to anthropogenic activities through urbanization and development near coastal areas (Creel, 2003). Reports from the Intergovernmental Panel on Climate Change (IPCC, 2007) indicate that coastal zones are some of the primary areas that will be impacted by climate change and environmental degradation (Anthony et al., 2009; Dolan and Walker, 2006; IPCC, 2007). In recent decades the Gulf Coast region has experienced an increase in the frequency of

natural disasters that are linked to global warming, sea level rise, and climate change (Twilley et al., 2001). Consequently, these events exacerbate the negative impacts of environmental degradation on coastal communities. (Petterson et al., 2006).

Similar studies have been conducted on the coastal landscape of Mississippi and Alabama using multi-temporal Landsat imagery. Ellis et al. (2011), investigated the Land Use and Land Cover (LULC) change of the Mobile Bay vicinity and their impacts on coastal environments, their study area consisted of Mobile and Baldwin Counties. O'Hara et al. (2003) conducted a LULC study from 1991 to 2000 to identify vegetation patterns and seasonal variability to improve the identification of urban land cover along the Mississippi Gulf Coast.

Although this study takes a similar approach to previous studies conducted in this region for classification methodology, I will use Landscape Metrics to enhance our understanding of the urban landscape development of this region and to better characterize the land cover change detection. Furthermore, I will use the landscape metrics to perform a comparative analysis of urban land cover between the five counties in the Gulf Coast region of Mississippi and Alabama.

1.2 Study Area

The study area consists of five coastal counties: Hancock, Harrison, and Jackson of Mississippi; and Mobile and Baldwin of Alabama. The area lies between 31.3° and 30.2° latitude, and -88.4° and -89.3° longitude (Fig. 1.1). The physical terrain of the study area is characterized by a coastal landscape that has a variety of wetlands including marshes and swamps that are adjacent to the coast. These wetlands extend inland along streams and rivers that are connected by watersheds and estuaries that drain into the Gulf

of Mexico. Coastal Mississippi is situated in the Pine Hills Physiographic Division and the Mississippi Delta Province of the Louisianian Biogeographic Region. It is characterized by Pine Hills areas that are typical of upland plains. These areas are dissected by streams forming regions of slopes (Oivanki, 1998). The Coastal Alabama lies within the East Gulf Coastal Plain Ecoregion and the Louisianan Marine Province. The U.S. Forest Service classifies the region as representing the Coastal Plains and Flatwoods within the Subtropical Division of the Humid Temperate Domain (Bailey et al., 1994). These physiographic and geomorphologic features create an environment that is very complex, sensitive and rich with biodiversity (Ennis et al., 2014).

In this study, 10 scenes for 8 different time periods were acquired to perform classifications (Table 3.1). Due to inconsistencies of Landsat imagery positions over 4 decades, the study area had to be trimmed to include the intersection of all the scenes used for this study. The result of this process is that 26% of Hancock County, 10% of Mobile County and 43% of Baldwin County are not included in the study results. However, this does not affect the overall results due to the consistent size of the study area. Fig. 1.1 is a map of the study area.

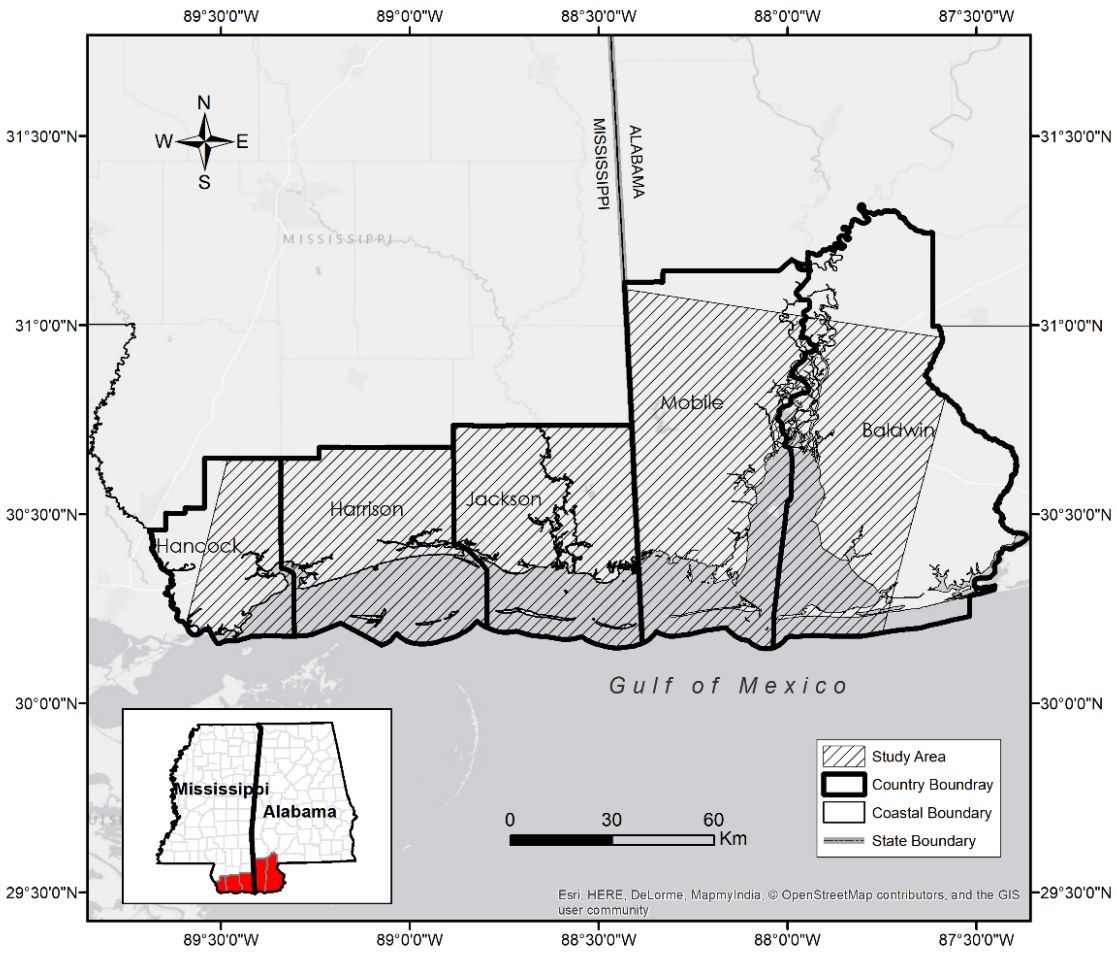

Figure 1.1 Map of Study Area

Hancock, Harrison, and Jackson Counties of Mississippi; and Mobile and Baldwin Counties of Alabama

1.3 Objectives

The objectives of this study are to provide a general thematic landscape change assessment of the lower counties of Mississippi: Jackson, Harrison, and Hancock and the lower counties of Alabama: Mobile and Baldwin. The outputs of this study also include long-term LULC maps for the years 1973, 1980, 1986, 1995, 2000, 2005, 2010, and 2015

for each county. Additionally, landscape metrics were used to assess the urban development for each county throughout the time period of the study.

1.4 Thesis Organization

This study is organized into five chapters. Chapter I is the introductory chapter which provides an overview of contents and the scope of the study. Chapter II is a literature review of the topics covered in this paper, which includes remote sensing and GIS, land cover change science and landscape metrics. Chapter III contains the methodologies used in this study and is divided into four sections: data acquisition, classification, change detection, and landscape metrics. Chapter IV contains the final results of the study which includes a comparison of the accuracies of three supervised classification methods, an overall accuracy assessment for all the classified images, change detection confusion matrices, urban landscape metrics assessments, and the time series of the classified images for each county. Chapter V is the conclusion and summaries of the result of the overall assessment of the land cover change and urban development for the study area in the past four decades.

CHAPTER II

LITERATURE REVIEW

2.1 Remote Sensing and Geographic Information Systems

Remote sensing is defined as the process of collecting information about the physical properties of objects based on the reflected or emitted electromagnetic radiation without coming into direct contact with it (Davis and Swain, 1978 p. 1). Colwell (1966) also defined remote sensing as "reconnaissance at a distance," referring to the way remote sensing is often used in the process of monitoring natural and anthropogenic processes on the Earth's surface over time. Information can be derived from remote sensing data that is collected by a variety of different sensors. These sensors are used to measure the reflected or emitted light (electromagnetic energy) in specific ranges of the electromagnetic spectrum (bands) from target areas in a specific field of view. Objects of interest such as vegetation, soil, buildings, or water bodies often exhibit a specific spectral profile detected by the different bands. These bands cover different wavelengths which include visible light, near infrared, microwaves, and radio waves (Jensen and Cowen, 1999).

Sensors on board earth-orbiting satellites became popular beginning in the 1960s. Advances in the space rockets and image capturing technology made it possible to launch space-born sensors on board a variety of satellites for military and civilian purposes (Williamson, 1997). Satellite remote sensors are used in monitoring natural processes in

earth systems such as weather and atmospheric interactions, ocean surface temperatures, phenology, and biogeochemistry (Lipp et al., 2001; Weng, 2002). Similarly, remote sensing is used to monitor human-environment systems such as urban development, climate change, and environmental pollution (Kolios and Stylios, 2013). Early satellite sensors were limited in their spectral and spatial resolutions and thus had limited capabilities due to their relatively small computational power along with the difficulty of transmitting and storing the large amount of data required by earth observation satellite (Jensen, 1986; Wulder et al., 2012).

In the early days of satellite remote sensing, sensors had low spatial resolution, such as the Moderate Resolution Imaging Spectroradiometer (MODIS) and Advanced Very High Resolution Radiometer (AVHRR), that were ideal for covering large areas with uniform land cover distribution (Lhermitte et al., 2008). By the 1970s, NASA introduced the Earth Resources Technology Satellite, which was eventually renamed the Landsat program and later operated by the United States Geological Survey (USGS) (Lauer et al., 1997). The Landsat satellite program had three significant impacts on remote sensing science. The first and immediate impact was that it provided the first systematic observation of Earth's land surfaces over an extended period of time. Next, it propagated interest in the digital analysis of remote sensing data in the broader natural science community due to its standard data format and accessibility through online databases that are available to the public free of charge. Thus, accelerating the development of new data processing methods and software packages to process the large amount of data available. Finally, the Landsat program served as a template for different

governmental and non-governmental organizations around the world to launch more Earth-observing satellites (Campbell and Wynne, 2011).

The first generation of the Landsat earth observatory satellites; Landsat 1, Landsat 2, and Landsat 3 all had the Multispectral Scanner (MSS) sensor with a 60 m spatial resolution and 4 spectral bands which included Green, Red, and 2 NIR bands. Landsat Thematic Mapper (TM) sensor was carried onboard Landsat 4 and Landsat 5 which had 30 m spatial resolution and 6 spectral bands (Blue, Green, Red, NIR, SWIR1, SWIR2) and 1 thermal band with 120 m spatial resolution. The Enhanced Thematic Mapper Plus (ETM+) sensor was carried on Landsat 7 which had the same 6 spectral and 1 thermal band as the TM sensor, but it also included a panchromatic band with 15 m resolution. In 2003, the ETM+ sensor onboard Landsat 7 experienced a malfunction in its Scan Line Corrector (SLC) which resulted in wedge-shaped omissions in the delivered images and significantly affected the quality of the data (Storey et al., 2005). Consequently, Landsat 5's operational life was extended to continue the acquisition of data for a continuous earth observatory data archive (Lauer et al., 1997; Wulder et al., 2012). Landsat 8 carried the Operational Land Imager (OLI) sensor, which had 11 spectral bands in total. Of the 11 bands, 9 bands have a spatial resolution of 30 meters, bands 1 to 7 (Ultra Blue, Blue, Green, Red, NIR, SWIR1, SWIR2) and band 9 (Cirrus). Landsat 8 also had a panchromatic band (band 8) which has a 15 m resolution, and a Thermal Infrared Sensor (TIRS) with 2 Thermal bands, band 10 and 11 that are 100 m resolution (Roy et al., 2014).

Geographic Information Systems (GIS) is a computer system for capturing, storing, analyzing, and displaying geospatial data. Geospatial data is a type of data which

has descriptive (attributes) and locational (geographic) information (Chang, 2006). Another way to interpreted GIS is GIScience, which is the science of "the development and use of theories, methods, technologies, and data for understanding geographic processes, relationships, and patterns" (Duckham et al., 2004). Application of GIS methods and tools are used in many different research fields such as natural resource management, forestry, wildlife ecology, meteorology, environmental analysis and monitoring, landscape analysis, temporal land cover change detection, urban planning, transportation, public health, political and demographic distribution, and many more.

Spatial data within GIS systems fundamentally changed the way scientist and professionals look at recorded information. The combination of spatial information data (location) and nonspatial-attribute (or descriptive) data makes it possible to visualize and interpret digital data to answer relevant questions and derive useful information from existing sources. The improvements in the capability of remote sensing and GIS systems are due to the increasing capacity of digital storage and processing power, and the enhancements in optical sensor technology. GIS and remote sensing provided tools and methodologies that can be used to augment and further increase the reach of scientific research. Therefore, GIS and remote sensing receive increasing interest from the scientific community, especially within the natural sciences (Turner et al., 2008). The combination of the cost-effective multispectral and multi-temporal data that is collected by remote sensors and the strong analyzing, storing, and displaying of digital data in the flexible environment of GIS can be a potent tool when used in the correct context (Crossett et al., 2004).

2.2 Land Cover Change Science

Land cover change science is an extensive research field that is in the business of understanding and monitoring the global system, land cover, and land use using remote sensing technologies (Samek et al., 2012). Studying ecosystems and anthropogenic effects on the environment became the central points of land cover science. From within this interest, the multidisciplinary research field of LULC science was born (Turner et al., 2008). LULC science attracts a variety of scientists from a variety of research fields which include remote sensing/GIS, signal engineers, natural sciences, political ecology, landscape ecology, resource economics, biogeography, forestry, social scientists and many more (Gutman et al., 2004; Riebsame et al., 1994; Turner et al., 2008). The primary goals of LULC science are to 1) monitoring land change throughout the world 2) modeling of land change, 3) understanding change as a coupled environmental-human element, and 4) evaluation of land sustainability, vulnerability, and resilience (Turner et al., 2008).

The advancement of remote sensing and the increased capacity and computational power of GIS contributed to the development of classification and change detection methods (Jensen, 2005). This advancement and availability of land imagery made it possible to conduct many LULC studies across the globe. Consequently, the need was crucial for a universal classification standard to make the finding of different research results usable across different fields. In 1976, the USGS published the first standardized LULC classification system in a professional document titled *Land Use and Land Cover Classification System for Use with Remote Sensor Data*. The document highlights three levels of land classification systems [level: I, II, III]. Each higher level is more specific

and has a higher number of land classifications than the previous one. This classification system became commonly known by its author's name, the Anderson land classification system (Anderson et al., 1976).

Researchers use a variety of different classification methods to identify LULC classes, the choice of classification methods depends on few factors. The subject of the research, the study area, availability of data, cost, and time constraints are few of the elements to have in mind when conducting a LULC research study (Weng, 2012). Classification methods fall under three general criteria: training samples, data distribution, and per-pixel (hard) or subpixel (soft) classification (D. Lu and Weng, 2007). Supervised classification methods use training sites to determine the spectral signature of each class. Training sites are locations of pixels with known land cover classes. The classification of each pixel is obtained through manual input using a digital pin in a GIS program. These points are referenced using aerial imagery, high-resolution satellite imagery, or field observations (Rogan and Chen, 2004). Supervised classifiers combine the spectral signature of all the training pixels that are assigned to each class to produce a combined signature. Great care is exercised to use training pixels that are representative of one class only to derive an accurate signature (D. Lu and Weng, 2007). The second criterion is data distribution. Parametric distribution assumes that the parameters (mean vector and covariance matrix) has a Gaussian distribution. One major drawback of parametric classifiers is the difficulty of integrating non-statistical information such as census data or elevation data, an example of a parametric classifier is the Maximum Likelihood Classifier (MLC) (Weng, 2012). Non-parametric classifiers make no assumption about the data distribution and therefore tend to have higher

accuracy due to the complexity of the parameters of most satellite data. (D. Lu and Weng, 2007; Paola and Schowengerdt, 1995). Some of the most popular non-parametric classifiers are Artificial Neural Networks (ANNs), Support Vector Machine (SVM), and Expert Systems (ES) (Weng, 2012).

Classification of satellite imagery is dependent on the quality of data and the specification of the sensors used to obtain that data. Spatial, spectral, and temporal resolution determine the amount of information that can be extracted from satellite imagery (Weng, 2012). Spatial resolution refers to the area one pixel covers on the ground, and it dictates the measurement of the smallest object that can be detected. To accurately detect an object using remote sensors, the spatial resolution must be at least one-half of the diameter of the smallest object to be detected (Jensen and Cowen, 1999). Spectral resolution is the number and the range of electromagnetic bands used by the sensor. Higher spectral resolution is required to identify different types of urban land cover due to the similarity in the materials and surfaces (Macleod and Congalton, 1998; Weng, 2012). Visible light (VIS), Near Infrared (NIR), Medium Infrared (MIR), and Panchromatic are all types of spectral resolutions that enable image analysts to discern between different types of materials and land surfaces with greater accuracy (Rogan and Chen, 2004). Temporal resolution refers to the amount of time it takes for the satellite to revisit the same spot on earth. Temporal resolution is essential for LULC change detection. The higher temporal resolution allows for a higher amount of data acquisition in the same geographic area, and it provides a better chance of acquiring imagery with a low amount of cloud cover (Lu et al., 2008).

Change detection methods are used to quantify the amount and type of change in the satellite imagery with two or more intervals. Post-Classification Processing (PCP), Image Differencing (ID), Principle Component Analysis (PCA), and Change Vector Analysis (CVA) are some of the popular change detection methods used in the literature (Coppin et al., 2004; Macleod and Congalton, 1998; Yu et al., 2012). PCP is a straightforward change detection method to implement and understand. It requires a before and an after classified image, next it assigns each pixel a new value by comparing the class of pixel from the first image to the class of the same pixel from the second image, and it creates a new raster dataset with "from-to" classes (e.g., from Forest to Urban). Image differentiation (ID) does not rely on pre-classifier imagery; it performs change detection by subtracting value from one band in the first image from the value of the same band in the second image. The result is a "from-to" raster with unchanged pixels set to zero. One disadvantage of ID is the difficulty of deriving the change detection matrix from the resulting raster data. Principle Component Analysis (PCA) method uses a confusion matrix to plot the first image against the second image with rows and columns having a change and no change sections. Change vector analysis (CVA) involves using two components: change of direction and change of magnitude. The change in direction is calculated using angular vectors, and the magnitude is calculated using Euclidian distance (Malila, 1980).

Recent approaches to classification of remote sensing imagery involve the use of machine learning techniques based on domain adaptation (DA) and transfer learning procedures. DA methods focus on using existing derived signatures to classify newly acquired imagery that has different acquisition conditions, which include different

sensors (number of bands, spatial resolution), different acquisition time period (sun angle and luminosity), or different geographical area. DA methods address the issue of collecting accurate and consistent classification signatures and ground truth data for each image, which is often time-consuming and expensive and is considered one of the biggest problems of supervised image classification (Tuia et al., 2016).

Similar LULC studies have been conducted in the Gulf Coast of Mississippi and Alabama. Ellis et al. (2011) studied the LULC change of the Mobile Bay vicinity and their impacts on coastal environments. Their study area consisted of Mobile and Baldwin Counties of Alabama. They found that the urban land cover increased by 7% between 1974 and 2008 and in the same period the upland herbaceous land cover decreased by 350 km^2. The result of their study was incorporated in the coastal conservation efforts by the Mobile National Estuary Program. O'Hara et al. (2003) conducted a LULC study to identify vegetation patterns and seasonal variability to improve the identification of urban land cover along the Mississippi Gulf Coast. Using Landsat imagery, they identified spectral changes between leaf-off and leaf-on variations to develop formal classification rules based on thematic-change logic tables. The result of their study is an increase in classification accuracy of more than 90% and a robust method to identify low-density urban development that can be difficult to detect due to the dense vegetation cover.

2.3 Landscape Metrics

Landscape metrics are a set of numeric measurements that quantify the spatial patterns of landscape compositions and configurations, which can be linked to ecological and anthropogenic processes. The application of landscape metrics has its origins in landscape ecology, with species-centric thinking as the phenomenon to be modeled.

Quantifying habitat fragmentation and understanding spatial patterns of population dynamics on small and large scales. (Ji et al., 2006).

Landscape metrics are calculated on the patch, class, and landscape level. A fundamental element of landscape metrics is that all landscapes are composed of a mosaic of patches (Urban and Shugart, 1987). A patch is a single unit of space that is defined by the phenomenon under investigation and can be described as a relatively homogeneous environmental condition where discontinuities distinguish the patch borders in the landscape relative to the phenomenon under investigation. Class (patch type) metrics are the statistical characteristics of all patches within a single class. These statistical characteristics describe first-order and second-order statistics such as area-weighted mean, median, range, standard deviation, or coefficient of variation. Landscape metrics describe similar statistics to class metrics but over the entire study area (Mcgarigal, 2001).

Landscape composition refers to several types of metrics which include the proportion of the landscape in each patch type, patch richness, patch evenness, and patch diversity. Landscape configuration refers to the physical distribution or spatial character of patches within the landscape. Some aspects of configuration, such as patch isolation or patch contagion, are measures of the placement of patch types relative to other patch types, the landscape boundary, or other features of interest. Other aspects of configuration, such as shape and core area, are measures of the spatial character of the patches (Mcgarigal, 2001).

Fragstats is a public domain computer program used in calculating landscape metrics and analysis of the distribution of spatial phenomenon from raster and vector

data. The program was developed at Oregon State University with collaborations from different academic and government organizations. A technical paper published by Fragstats authors describes the program and its capabilities in detail (McGarial and Marks, 1995).

Studies have been conducted using landscape metrics to quantify urban sprawl and develop cause and effect of the urbanization processes. Ji et al. (2006) used landscape metric to explore the general trends of urban sprawl of the Kansas City metropolitan area during the past 3 decades using classified Landsat imagery. They analyzed landscape metrics across several jurisdictions, metropolitan, county, and city and found that the city area scale is too narrow to describe the general trends of urban sprawl and found that the metropolitan area scale is too large. The county scale has a variety of different land covers and usually has a central urban core that can be characterized by patch density metrics. They also devised land consumption indices that identified observed increase in urban land cover to the increase in residential and commercial construction as the main driving forces for urban sprawl.

Herold et al. (2002), used landscape metrics to describe the urban structure that resulted from the land cover change based on mapped and classified aerial imagery of Santa Barbra, California. The result of their study shows that the landscape metrics can be useful in characterizing and segmenting homogenous regions of the urban land cover into different density types and land use types, which is often very difficult to do when looking at high-density urban environments.

CHAPTER III

METHODOLOGY

3.1 Data Acquisition

Landsat data is available through the USGS data repository EarthExplorer (USGS, 2017a) and it was the primary data source in this study. EarthExplorer provides users with the ability to search, view, and order a variety of satellite imagery, aerial photography, and cartographic products, most of which are free of charge. EarthExplorer tools provide users with the ability to specify a location, date (start/end), cloud cover, and datasets. Location is expressed using addresses, path/row, coordinates, or an area drawn manually on a reference map. The search query can be set with a start and an end date. Similarly, it can also be specified by one month with multiple years. EarthExplorer also provides an advanced search method to refine satellite imagery by the percentage of the area covered by clouds (Turner et al., 2008). Cloud cover on satellite imagery can result in erroneous outcomes due to the introduction of the cloud molecules' spectral signature in the pixels, which can result in a misrepresentation of the pixel classification (Zhang et al., 2002).

Landsat satellite series provide an unprecedented archive of earth surface land imagery with medium spatial resolution, and it has a 16-day revisit time. Therefore, Landsat imagery is ideal for conducting research on LULC detection and time series analysis. The availability of such large amounts of data and the ease of acquiring it

contributed significantly to the LULC science (Roy et al., 2014). In this study, 10 scenes for 8 different time periods are acquired to perform classifications (Table 3.1). The Landsat scenes acquired for this study are split into two categories: Multispectral Scanner (MSS) scenes and non-MSS scenes. Landsat 1, 2, and 3 (MSS scenes) use World Wide Reference System WRS-1 (Fig. 3.1) and Landsat 4, 5, 7, and 8 use WRS-2 (Fig. 3.2). WRS divides the Earth surface area observable by Landsat satellites into a grid of rectangles with an area of approximately 32,000 km^2 or 1.5 degrees by 1.5 degrees (Arvidson et al., 2006). Due to misalignment of WRS*1 and WRS-2, 2 scenes per year for the MSS scenes were used (path/row 022/039 & 023/039) and just 1 scene per year for the non-MSS scenes (path/row 021/039) to cover the study area. The MSS senses are classified separately and then mosaicked post classification to avoid misclassification by using the same signature for two different scenes. To avoid leaf-on leaf-off spectral inconsistencies, only scenes from the leaf-off season were used (October to February). Given the region's subtropical climate, the summertime has frequent cloud cover which can result in clouds covering the study area rendering the image unusable.

Table 3.1 Landsat Multispectral Image Data Acquired

Date	Satellite	Sensor	Spatial Resolution	Path/Row	# Bands
Oct. 30 1973	Landsat 1	MSS	60 m	022/039	4
Dec. 03 1973	Landsat 2	MSS	60 m	023/039	4
Oct. 29 1979	Landsat 2	MSS	60 m	022/039	4
Nov. 08 1980	Landsat 2	MSS	60 m	023/039	4
Jan. 31 1986	Landsat 5	TM	30 m	021/039	7
Oct. 17 1995	Landsat 5	TM	30 m	021/039	7
Oct. 28 2000	Landsat 7	ETM+	30 m	021/039	8
Oct. 18 2005	Landsat 5	TM	30 m	021/039	7
Oct. 16 2010	Landsat 5	TM	30 m	021/039	7
Oct. 14 2015	Landsat 8	OLI	30 m	021/039	11

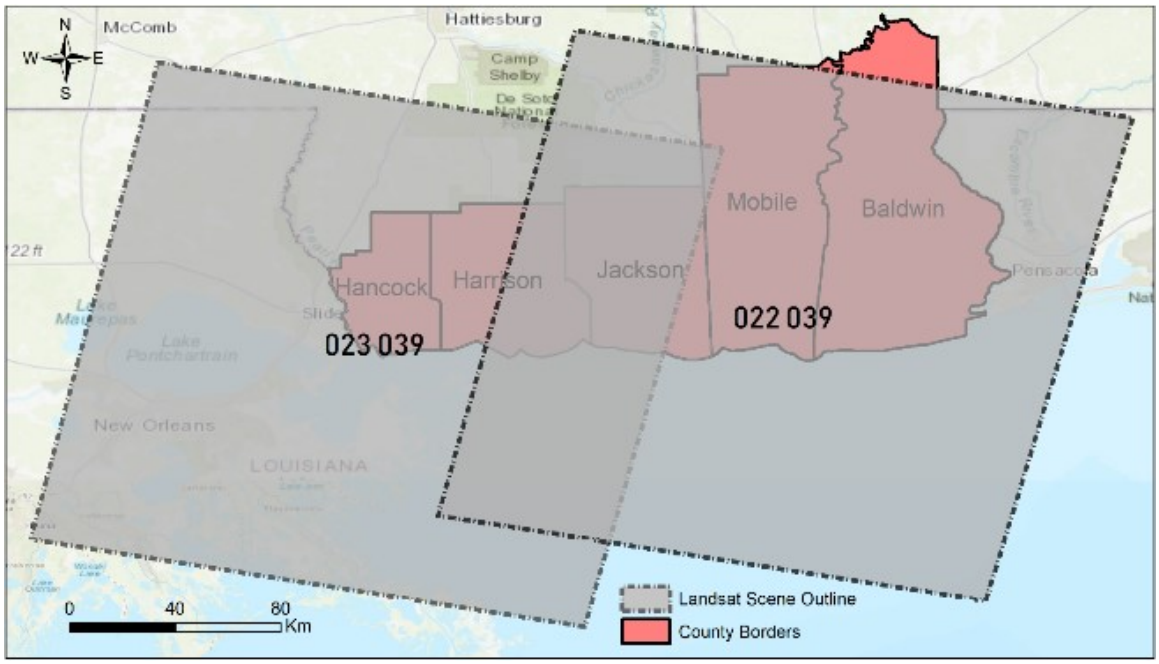

Figure 3.1 MSS scenes using WRS-1 reference system

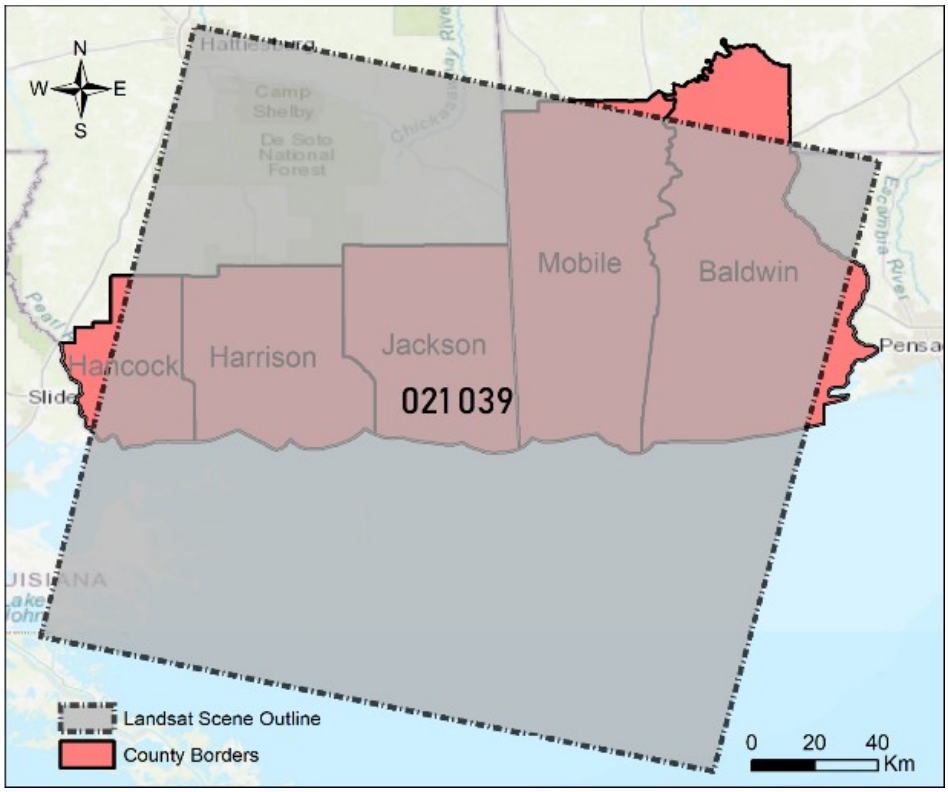

Figure 3.2 Non-MSS scenes using WRS-2 reference system

3.1.2 Preprocessing

Landsat MSS scenes were atmospherically corrected using Dark Object Subtraction (DOS) method. DOS assumes the existence of completely dark objects in a multispectral image, and it subtracts the value of the pixel with the lowest brightness value from the entire image and attributing the atmospheric effects to that value (Chavez, 1989). Finally, after the atmospheric correction was completed, the MSS bands were stacked from each scene to form a multi-band rasters to facilitate the classification process.

Landsat level-2 Surface Reflectance data products were used for the non-MSS scenes. These images are produced by the Earth Resources Observation Sciences (EROS) Center using their Ecosystem Disturbance Adaptive Processing System (LEDAPS). This specialized program produces atmospherically corrected images by applying Moderate Resolution Imaging Spectroradiometer (MODIS) atmospheric correction routines to Landsat scenes. The result of this process includes Surface Reflectance (SR), Top of Atmosphere (TOA) and several other quality assessment products (USGS, 2017b).

To ensure proper and accurate change detection results, all scenes were resampled to 30-meter spatial resolution and geometrically co-registered to the 2015 scene using ArcMap Georeferencing tool. RMS errors from the Ground Control Points (GCP) in the Georeferencing process were kept at less than 0.004meters for all scenes corrected. Next, visual inspection was performed by masking out irregularities such as cloud cover, cloud shadows, striping or bad lines that might return false classification. Finally, all scenes were clipped to the study area boundaries to reduce rendering and processing time.

3.2 Classification

By studying the area and performing several unsupervised classifications, the classification scheme used in this study contains 7 classes derived from a modified version of the Anderson level I classification scheme (Anderson et al., 1976). The classes include the following categories: Built-up/Urban, Agriculture, Forest, Rangelands, Marshes, Barren, and Water. The urban class represents anthropogenic landscapes which consist of residential areas, commercial districts and industrial parks, highways, and transportation hubs; the agriculture class includes open pasture and cultivated crops; the forest class includes deciduous, evergreen, mixed forests, and woody wetlands; the rangeland class includes scrub, grasslands, and forests in early stages of development; the marshes class consist of wetlands with low-density vegetation; the barren class includes beaches, strip mines, gravel pits or any areas with bare soil; the water class includes all bodies of waters such as oceans, lakes, and rivers. To make the classifications understandable and familiar, the colors of the classes are similar to the legend used in the National Land Cover Data (NLCD) (Homer et al., 2007).

3.2.1 Signature Training

Several supervised classification methods were tested to determine which would be the most appropriate for the parameters of this study. Supervised classification is performed by selecting user-identified pixels or a group of pixels and developing the spectral histogram from all the bands in the composite image; this histogram is then used to derive a signature. A robust signature for each class is calculated by combining the signatures of multiple training sites that are distributed across the image. This process is conducted by using two commercial GIS software, Erdas Imagine, and Esri ArcMap. The

signatures for each classification were derived using a stratified random approach by overlaying a 20 km^2 grid over the image and selecting training sites in each grid box for each class. We found this method to be quite useful in ensuring proper distribution of training sites over the entire image. However, this method of distribution may have some bias in urban classes because they tend to be concentrated in specific areas and some grids did not have any urban class cover. In such cases, the placing of two or more training areas in the grid adjacent to the empty grid was implemented. Li et al. (2015), in their long-term LULC study, used a similar number of training samples in each scene to reduce sampling bias in their class signature. Therefore, a similar number of pixels for each class in each scene was kept.

3.2.2 Supervised Classification Methods

Three supervised classification methods were identified as the most prominent classification methods used in the literature: Maximum Likelihood Classifier (MLC), Random Forest (RF), and Support Vector Machine (SVM). Many studies in the literature compared supervised classification methods (Hepner et al., 1989; Rozenstein and Karnieli, 2011; Singh, 2017). Maximum Likelihood Classifier (MLC) is a parametric supervised per-pixel (hard) classifier. It assumes the data is normally distributed and it uses the mean vector and covariance matrices as key input to estimate and assign each pixel to a specific class (Ahmad and Quegan, 2012; Rogan and Chen, 2004). Random Forest (RF) classifier (also called Random Trees) is a non-parametric classifier that does not require a priori knowledge of the data distribution. Random Forest works by collecting individual decision trees where each tree is generated from different samples and subsets of the training data so that for every pixel that is classified, a number of

decisions for its classification are made in rank order of importance. When graphed out it the graph can resemble a tree with branches and roots and offshoots. Next The data is recursively divided down the decision tree according to the defined classification framework. RF is known to be a more advance classification algorithm, but the classification accuracy is affected by multiple factors including pruning, boosting and decision thresholds (Otukei and Blaschke, 2010). The SVM supervised classification mothed is a non-parametric statistical that developed by machine learning research and it is built around the algorithm of maximizing the distance between different classes in a hyperplane, by increasing the distance between classes the classification insures a better separability between classes (Nemmour and Chibani, 2006).

In this paper, we conducted our classification assessment using separate training areas and accuracy points and we found that they often produce different results depending on the location, data, signature acquisition technique and visual inspection. Therefore, three scenes were chosen to perform all three supervised classification methods, and they were tested by using randomly stratified accuracy points to get the overall accuracy and the kappa coefficient (more on accuracy in 3.2.3). After preforming all three classifications using the same scenes we found that SVM has the highest overall accuracy and kappa coefficient, see (Table 4.1). Visual inspection also shows that SVM had the lowest number of misclassifications. SVM classification method is also shown to have higher accuracy results by other comparative studies (Foody and Mathur, 2004; Nemmour and Chibani, 2006).

3.2.3 Classification Accuracy

The number of accuracy points was calculated using the method outlined by Fitzpatrick-Lins, (1981) using the following equation:

$$N = Z^2 pq/E^2, Z=2$$

where N is the number of samples, Z is the generalized standard deviation value of 1.96 based on the two-sided confidence interval of 95 percent, p is the expected percent accuracy of 85 percent, q is 100 – p, and E is the allowable error. The expected percent accuracy, *p,* was based on the guidelines outlined by Anderson et al. (1976), which states that classification of remote sensing data must have a minimum of 85% accuracy. Due to the minimum field-based reference points, allowable error E was kept at 4 percent. Using this method, the number of accuracy points for each scene N is equal to 306 points, and the result was rounded to 300 points. The distribution of the accuracy points was based on equalized stratified random categorical distribution, where the number of accuracy points is divided equally among each class. The rationale behind this decision is that the study area has water bodies that make up a large percentage of the study area, and the urban class only represents about 5-10 percent of the study area. Stratified random categorical distribution is ideal because it combines the statistical properties of random distribution and ensures the representation of all classes in the accuracy matrix (Congalton, 1991; Fitzpatrick-Lins, 1981). After producing the accuracy points in each scene, they are verified visually using NAIP high-resolution aerial imagery and Digital Raster Imagery (DRI) (NRCS, 2008). Google Earth was used to verify accuracy points for the years where there was no aerial imagery available. NLCD LULC datasets were used as a reference for the scenes with the same year (Homer et al., 2004).

There are several methods to assess the classification accuracy. The most popular methods used in the literature are confusion matrices and Kappa coefficients (D. Lu and Weng, 2007). A confusion matrix is implemented by comparing each class with ground truth data; each class has a column with the number of correct and incorrect classifications compared against the ground truth data. Several accuracy measurements can be calculated from confusion matrices, which include producer's accuracy, user's accuracy, overall accuracy and the Kappa coefficient. Producer's accuracy indicates errors of omission in each class, and it can be calculated by dividing the total number of correctly classified pixels by the number of reference pixels. The user accuracy indicates an error of commission, and it can be calculated by dividing the number of correctly classified pixels by the total number of pixels classified in that category. The overall accuracy is the percentage of the total sum of the correctly classified pixels in each class divided by the total number of pixels in the matrix (Congalton, 1991). The Kappa Coefficient of Agreement is a robust method that is used extensively in measuring the accuracy of thematic classifications. It also takes into account the agreement of error matrices and chance agreement. The Kappa coefficient has a range from 0-1, where 1 indicates that classification accuracy is significantly better than random chance, and 0 indicates that classification accuracy is equal to a chance agreement (Hudson and Ramm, 1987; Rosenfield and Fitzpatrick-Lins, 1986). ArcMap was used to generate the confusion matrices to calculate the user's accuracy and producer's accuracy for each class, and the overall accuracy and the Kappa coefficient for each scene (Tables 4.1 and 4.2).

3.3 Change Detection

Given that supervised classification methods contain accuracy errors, a hybrid model of supervised classification and unsupervised change detection was chosen. Post-classification change detection method is used to quantify the LULC change between each pair of consecutive years. The process is conducted by comparing each pixel in the first classified image to the pixel of the second classified image with the same location; this process creates a "from-to" change detection matrix. The result is then displayed in a matrix with one year representing the rows and the other year representing the columns. The diagonal of the matrix represents no change, while other cells represent the LULC change of different categories.

For the unsupervised change detection, a variety of image differencing methods were tested to provide a change/no-change mask for each pair of time periods (Table 3.2).

Table 3.2 Image Differing Methods used in the Unsupervised Change Detection

Index	Name	Equation
NDVI	Normalized Difference Vegetation Index	(NIR – Red)/(NIR + Red)
NDWI	Normalized Difference Water Index	(NIR – SWIR) / (NIR + SWIR)
NDBI	Normalized Difference Built-up Index	(SWIR – NIR) / (SWIR + NIR)
RVI	Ratio Vegetation Index	NIR / Red
SAD	Spectral Angle Difference	(Kruse et al.,1993)

The Spectral Angle Diffrence (SAD) is a spectral change detection tool avalible through a comercial GIS software, ENVI under its change detection workflow. SAD works by detecting the difference of spectral angle between T-1 and T-2 pixels by measuring the angle between the vectors of the two spectra in each corresponding band

(Kruse et al.,1993). Using visual inspection of the original imagery, SAD combined with iterative threshold testing was found to give the best result for detecting the changed pixels. Subsequently, a change/no-change raster mask was produced for each pair of consecutive years in the study. This mask is then applied to a traditional post-classification comparison where only the pixels that were identified as changed pixels are included in the change detection matrix. This hybrid change detection model has the potential to reduce misclassification errors from being reflected in the change detection matrix (Megahed et al., 2015).

3.4 Urban Landscape Metrics

Multiple landscape metrics were used to describe the change in the urban/built-up classification by using complementary indices. Properties of growth and spread pattern were calculated to compare the urban development of counties across the time scale of this study. This type of comparison allowed us to compare the development of urban and impervious surfaces change/growth between counties. This section will attempt to describe each index that was used and its relevance to characterizing urban landscapes. Table 3.2 provides a summary of these indices.

Percentage area of landscape (PLAND) – area (ha) provides the percentage of each patch type (class) within the landscape. PLAND is one of the simplest landscape indices in that it allows for a general understanding of the proportion of each class in the entire landscape. Edge density (ED) index represents the sum of lengths of all edge segments within the patch type divided by the area total length (m), and it is measured in (m/ha) therefore it can be used to compare landscapes with different area sizes. Class Area (CA) represents the area for each class in the landscape. The Number of Patches

(NP) represents the number of patches for landscape or in each class; a higher NP number means that the patches are smaller and more fragmented, while a lower number means that the patches are more consolidated. Fractal dimension indices are based on perimeter-area relationship and are often used in landscape ecological research to measure the complexity of patch shape within the habitat landscape (Turner and Ruscher, 1988). Herold et al., (2002) used the area weighted fractal dimension index (AWMPD) to characterize the fragmentation of urban environments by measuring the complexity of patch shapes in the urban classes. A newer version of Fragstat renamed this index to area-weighted mean patch fractal dimension (FRAC_AM). Largest patch index (LPI) is the percentage of the landscape comprised of the single largest patch, the increase of LPI emphasizes the proportion growth of the total landscape area comprised of the largest urban patch. Euclidian Mean Nearest Neighbor Distance (ENN_MN) is the distance mean value over all urban patches to the nearest neighboring urban patch, based on shortest edge-to-edge distance from cell center to cell center. (Megahed et al., 2015).

Figure 3.3 shows the methodology flow chart. The first step was to acquire and preprocess the satellite data. Next, the imagery is made into an input for two main processes: supervised classification and the unsupervised change detection. The supervised classification yields the SMA classified maps for each time period. The unsupervised change detection yields the change/no-change masks. The SMA classified maps are combined with the change/no-change masks to create the change detection matrices, and they are also made as an input into FRAGSTATS to derive the Landscape Metrics.

A summary of landscape metrics used in this study

Metrics	Description	Units	Range
PLAND - Percentage of Landscape	equals the sum of the areas (m^2) of all patches of the corresponding patch type, divided by total landscape area (m^2), multiplied by 100	Percent	$0 < PLAND \leq 100$
NP- Number of Patches	equals the number of patches of the corresponding patch type (class).	None	$NP \geq 1$, without limit.
ED - Edge density	ED equals the sum of the lengths (m) of all edge segments involving the corresponding patch type, divided by the total landscape area (m), multiplied by 10,000 (to convert to hectares).	Meters per hectare	$ED \leq 0$, without limit
FRAC_AM - Area-weighted mean patch fractal dimension	FRAC equals 2 times the logarithm of patch perimeter (m) divided by the logarithm of patch area (m); the perimeter is adjusted to correct for the raster bias in the perimeter.	None	$1 \leq FRAC\_AM \leq 2$
LPI - Largest Patch Index	The area of the largest patch of the corresponding patch type divided by total area covered by urban.	%	$0 < LPI \leq 100$
ENN_MN - Euclidian Mean Nearest Neighbor Distance	The distance mean value over all urban patches to the nearest neighboring urban patch, based on shortest edge-to-edge distance from cell center to cell center.	Meters	$EMN\_MN > 0$, no limit
CONTAG- Contagion Index	Measures the overall probability that a cell of a patch type is adjacent to cells of the same type.	%	$0 < CONTAG \leq 100$

Landscape metrics descriptions from (McGarial and Marks, 1995)

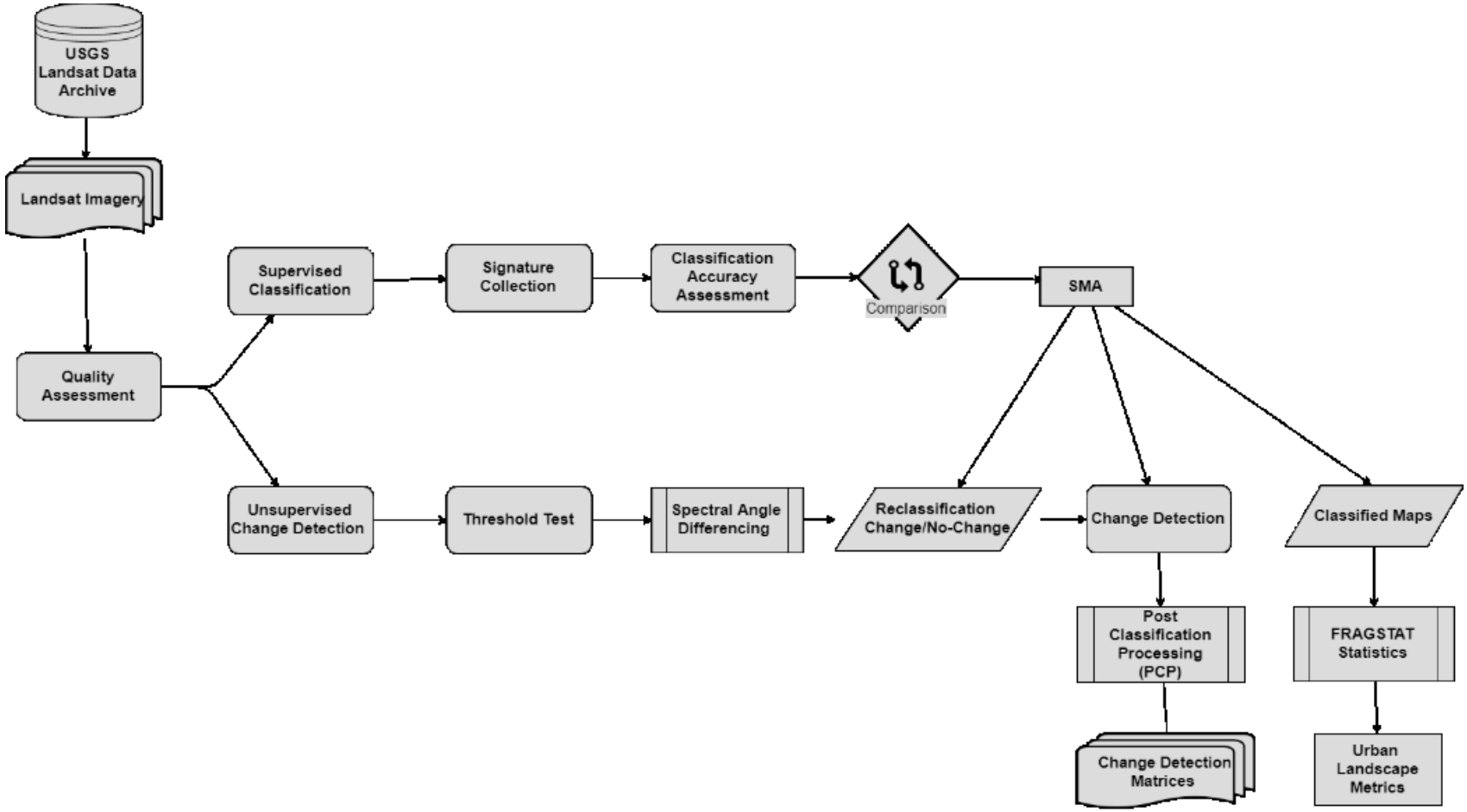

Figure 3.3 Methodology Flow Chart

CHAPTER IV

RESULTS

4.1 Classification Results

4.1.1 Classification Methods Comparison

Before choosing a supervised classification method, three methods were tested: Maximum Likelihood Classifier (MLC), Random Forest (RF), and Support Vector Machines (SVM). The accuracy tests were conducted on three different years 1973, 2000, and 2015. SVM had the highest accuracy values. SVM also proved to be a better classifier from a qualitative viewpoint, as it had significantly fewer problems with the "salt-and-pepper" issues, which can result in scattered patches of small sizes that are comprised of 1 or 2 isolated pixels. The effects of this problem need to be reduced because it can potentially reduce the effectiveness of patch metrics to analyze landscape patterns. Another factor for choosing SVM is that throughout the accuracy testing phase, SVM did not need as many training sites as MLC to get similar results, and it performed significantly faster than the RF method.

Table 4.1 Supervised Classification Accuracy Comparison

	MLC		RF		SVM	
	Overall %	**Kappa**	**Overall %**	**Kappa**	**Overall %**	**Kappa**
1973	77.95	0.750747	74.76	0.715041	81.04	0.77446
2000	77.51	0.742581	78.44	0.753172	87.91	0.85652
2015	81.42	0.789303	82.016	0.79623	92.29	0.90734
Average	**78.96**	**0.760877**	**78.41**	**0.754814**	**87.08**	**0.84611**

4.1.2 Classification Accuracy

The average overall accuracy for all the SVM classified maps is 85% ± 6.34, which according to Anderson et al. (1976) meets the accuracy requirements for LULC studies. During the change detection phase, 4x4 majority aggregation was used on the classified maps to reduce the salt-and-pepper problem. Coincidentally, post aggregation maps were found to have 1-3% higher accuracy than the none-aggregate maps. Given that the aggregate maps were used for the change detection, the accuracy figures were used for the aggregate maps as well. The average Kappa coefficient was 0.82 ± 0.08. These values indicate that all of the classified maps have classification accuracy that is better than random chance agreement. The scene with the highest accuracy is the 2015 scene; the higher accuracy may be attributed to the OLI sensor's higher spectral and radiometric resolution. Although, the OLI and TM sensors have the same spatial accuracy, it was significantly easier to identify features in the OLI scene during the signature training phase that may be due to the higher radiometric resolution of OLI. The higher quality signatures obtained from the OLI scene maybe also contribute to its higher overall

accuracy. Table 4.2 shows the producer's accuracy (errors of omission), user's accuracy (errors of commission), the overall accuracy, and the Kappa coefficient for each classified map.

Table 4.2 SVM Classification Accuracy

Scene (Year)	Average Producer's Accuracy (%)	Average User's Accuracy (%)	Overall Accuracy (%)	Kappa coefficient
10-30-1973 + 12-03-1973 MSS	82.27	80.23	81.04	0.77446
10-26-1979 + 11-06-1980 MSS	83.33	80.43	81.20	0.77689
01-31-1986 TM	87.19	87.20	87.47	0.85190
10-17-1995 TM	83.29	83.24	83.75	0.80766
10-28-2000 ETM+	87.72	88.55	87.91	0.85652
10-18-2005 TM	75.21	76.45	79.61	0.75462
10-16-2010 TM	81.30	81.65	82.74	0.79418
10-14-2015 OLI	91.33	91.40	92.29	0.90734
Average	**84.34**	**84.75**	**85.63**	**0.82870**

4.2 Change Detection Matrices

The change detection matrices were derived by combining the raster dataset of each consecutive classified years and then using the change/no-change raster derived from the SAD as a mask for the no-change pixels. The output table of the combined raster is then used in a pivot operation to produce the number of changed pixels in each class. The number of pixels is then converted to area in km^2 using this formula:

*Number of pixels * 30 meters * 30 meters * 0.000001 km^2/$meter^2$*

The diagonal values in matrix table represent the unchanged area, and they are derived from the supervised classification maps. The non-diagonal values represent the change of each class (row) into a different class (column), see Tables 4.3 to 4.9 for results.

4.3 Overall Land Cover Change Assessment

Over the last four decades, the land cover of the Gulf Coast counties of Mississippi and Alabama have experienced a significant change in all land cover types. The general trend of the percent land cover change is summarized in Table 4.10. The urban/built-up land cover which includes impervious surfaces doubled in size and resulted in an overall increase of 4.8% or approximately 660 km^2 between 1973 and 2015 with the Rangeland and Agriculture land covers absorbing most of the urban expansion. On the other hand, Agriculture and Rangeland land cover classes have experienced a decrease of 2.33% or 310 km^2 and 9.2% or 1230 km^2 respectively. The Marshes land cover changed with a decrease in area size of 1% or 140 km^2. The Barren and Water land cover classes both remained relatively stable with a slight increase in area 0.15% or 20 km^2 and 0.5% or 60 km^2 respectively.

At the study area scale, the urban land cover increased over the past four decades at an average rate of 1.68% per year, and the Agriculture and Rangeland cover bore the majority of urbanization. Other metrics were used to describe the continuous urban expansion over the study period. Class Area (CA) and Number of Patches (NP) indicate a general uptrend with the most dramatic increase happening between 1973 and 1986, indicating a higher urbanization rate in the early years during that period, and rate declining in urban land cover thereafter. The increase of LPI emphasizes the proportion

growth of the total landscape area comprised of the largest urban patch. By contrast, ENN_MN dipped from 1973 to 1995 and then remained steady to 2015. We infer from this fluctuation in value that the space between urban neighborhoods is shrinking over time as a result of higher urbanization density. FRAC_AM climbed between 1973 and 1986, and later it decreased sharply thereafter, which means that the level of complexity and fragmentation increased for the landscape patches until 1986 and then it gradually became less fragmented; we attribute this observation to the urban "fill-in" effect. The drop in CONTAG values between 1973 and 1980 may have resulted from higher fragmentation. However, the sharp reversal indicates the consolidation of urban patches.

Next, we identified the landscape effects and spatial patterns of built-up land expansion. As a general trend, the Rangeland cover patches became more fragmented as a result of the increase of built-up area over the period of this study as indicated by the negative correlation between the Built-up/Urban PLAND and Rangeland LPI ($r = -0.706$, $p < 0.05$). Agriculture land cover had a smaller correlation at ($r = -0.5294$). There was a small and statistically insignificant correlation between the Forest land cover patches and urban expansion ($r = -0.2183$). Statistical analysis suggests that Rangeland aggregation indices had the highest negative correlation with the area of built-up land in places that are highly developed, indicating the increased fragmentation of Rangeland, which is a characteristic of urban sprawl and expansion of residential low-density establishments away from the urban core. Although there is a negative correlation between agriculture and forestland, the effect is less severe.

4.4 Urban Land Cover Assessment by County

Comparing the landscape of the counties, Baldwin County was found to have the highest average rate of urban development at 2.35% per year, followed by Mobile County at 2.31% per year, Hancock County at 2.04%, Harrison County at 1.51% per year, and finally, Jackson County at 1.37%. The LPI and PLAND indicate that Jackson County has the highest level of fragmentation given by the correlation of rangelands and expansion of urban land cover at ($r = -0.79$, $p < 0.01$), followed by Baldwin County ($r = -0.666$, $p < 0.01$), Mobile County ($r = -0.63$, $p < 0.01$), Harrison County ($r = -0.61$, $p < 0.01$) and finally Hancock County ($r = -0.274$). The increase of Edge density indicates the total length of the edge of the urban patches due to land use fragmentation (m/m^2). Hancock County had the highest level of ED at an average of 38.47 m/m^2 which supports the conclusion that Hancock County has the highest aggregation index (aggregation is opposite fragmentation). Looking at the Euclidian Nearest Neighbor Mean Distance (ENN_MN) index, there is no substantial difference between counties and all of them follow the general trend where the space between urban neighborhoods shrink over time, which is a result of higher urbanization density.

Table 4.3 2015 – 2010 Change Detection Matrix

	2010						
2015	Urban	Agriculture	Forest	Rangeland	Marshes	Barren	Water
Urban	**834.95**	19.93	18.18	24.7	9.08	10.68	8.68
Agriculture	7.33	**524.09**	14.69	41.49	0.35	2.25	0.05
Forest	42.78	26.53	**4702.51**	237.76	6.69	0.36	0.26
Rangeland	17.4	63.3	148.26	**377.61**	1.95	2.34	0.17
Marshes	1.13	0.17	4.77	1.54	**268.75**	0.33	10.07
Barren	1.95	3.59	2.1	1.26	0.57	**45.88**	3.92
Water	0.3	0.13	0.3	0.17	5.76	5.79	**3849.08**

Values represent area in km^2

Table 4.4 2010 – 2005 Change Detection Matrix

	2005						
2010	Urban	Agriculture	Forest	Rangeland	Marshes	Barren	Water
Urban	**854.31**	6.47	43.08	51.81	31.71	4.01	1.63
Agriculture	18.92	**492.45**	38.01	68.13	2.31	3.24	0.36
Forest	22.85	3.39	**4626.45**	157.19	27.75	0.17	1.15
Rangeland	18.95	38.37	152.09	**469.26**	19.9	1.55	0.58
Marshes	4.01	0.33	7.02	2.71	**275.11**	0.5	12.93
Barren	4.78	2.47	6.05	4.26	1.12	**53.66**	6.59
Water	1.51	0.13	1.54	0.63	5.2	2.25	**3886.06**

Values represent area in km^2

Table 4.5 2005 – 2000 Change Detection Matrix

	2000						
2005	Urban	Agriculture	Forest	Rangeland	Marshes	Barren	Water
Urban	**673.66**	15.91	56.07	20.52	3.47	4.82	1.24
Agriculture	2.85	**448.04**	13.66	44.43	0.17	2.12	0.02
Forest	8.34	14.92	**4746.74**	148.35	13.01	3.95	0.44
Rangeland	21.84	44.45	279.64	**425.9**	6.66	4.07	0.19
Marshes	11.43	1.22	68.31	7.68	**268.45**	2	2.13
Barren	2.57	2.74	9.56	3.2	0.78	**48.94**	4.42
Water	2.57	0.82	2.23	2.66	14.09	7.18	**3881.47**

Values represent area in km^2

Table 4.6 2000 – 1995 Change Detection Matrix

	1995						
2000	Urban	Agriculture	Forest	Rangeland	Marshes	Barren	Water
Urban	**602.04**	8.71	67.23	11.68	9.5	4.6	3.7
Agriculture	25.61	**563.03**	58.15	44.15	10.27	3.34	1.1
Forest	23.34	21.68	**4721.22**	120.11	17.25	1.63	2.27
Rangeland	32.55	68.93	305.72	**312.62**	27.06	2.54	3.96
Marshes	3.98	1.42	22.25	1.83	**271.42**	4.52	14.81
Barren	8.23	4.15	12.08	4.31	2.78	**49.39**	5.58
Water	0.33	0.11	1.24	0.29	6.83	55.39	**3779.94**

Values represent area in km^2

Table 4.7 1995 – 1986 Change Detection Matrix

	1986						
1995	Urban	Agriculture	Forest	Rangeland	Marshes	Barren	Water
Urban	**548.26**	30.53	15.21	46.52	14.15	1.14	1.52
Agriculture	14.67	**613.67**	15.86	53.05	4.12	3.7	0.24
Forest	92.92	94.42	**4084.09**	491.67	162.21	2.18	5.06
Rangeland	2.99	26.51	63.78	**187.32**	1.77	0.83	0.94
Marshes	9.7	15.02	11.12	17.43	**299.5**	0.55	5.85
Barren	1.57	0.8	3.41	0.52	2.42	**38.33**	3.56
Water	2.43	0.22	1.58	0.71	8.45	2.35	**3778.32**

Values represent area in km^2

Table 4.8 1980 – 1973 Change Detection Matrix

	1973						
1980	Urban	Agriculture	Forest	Rangeland	Marshes	Barren	Water
Urban	**279.01**	21.87	39.95	33.32	4.49	0.99	1.98
Agriculture	24.25	**574.12**	50.88	93.54	5.11	0.41	0.14
Forest	3.77	3.11	**3735.18**	2.14	1.27	0.03	0.37
Rangeland	10.55	16.32	154.83	**1086.06**	2.32	0.3	0.13
Marshes	6.73	6.43	107.31	26.49	**294.93**	0.57	8.41
Barren	9.37	4.46	4.62	5.52	0.75	**41.99**	12.11
Water	4.16	0.92	6.47	1.62	19.05	8.78	**3786.16**

Values represent area in km^2

Table 4.9 2015 – 1973 Change Detection Matrix

	1973						
2015	Urban	Agriculture	Forest	Rangeland	Marshes	Barren	Water
Urban	**336**	171.78	319.15	368.38	35.86	15.39	21.84
Agriculture	67.22	**342.14**	89.03	193.75	9.69	0.83	0.31
Forest	123.86	261.99	**3989.77**	1323.67	123.19	2.42	5.44
Rangeland	76.87	217.38	371.31	**382.63**	35.37	2.53	1.01
Marshes	13.6	4.76	50.13	23.69	**238.17**	0.49	16.09
Barren	12.37	12.02	15.53	12.75	2.23	**23.82**	8.46
Water	13.23	2.28	21.38	4.99	48.92	22.09	**3774.63**

Values represent area in km^2

4.5 Urban Landscape Metrics

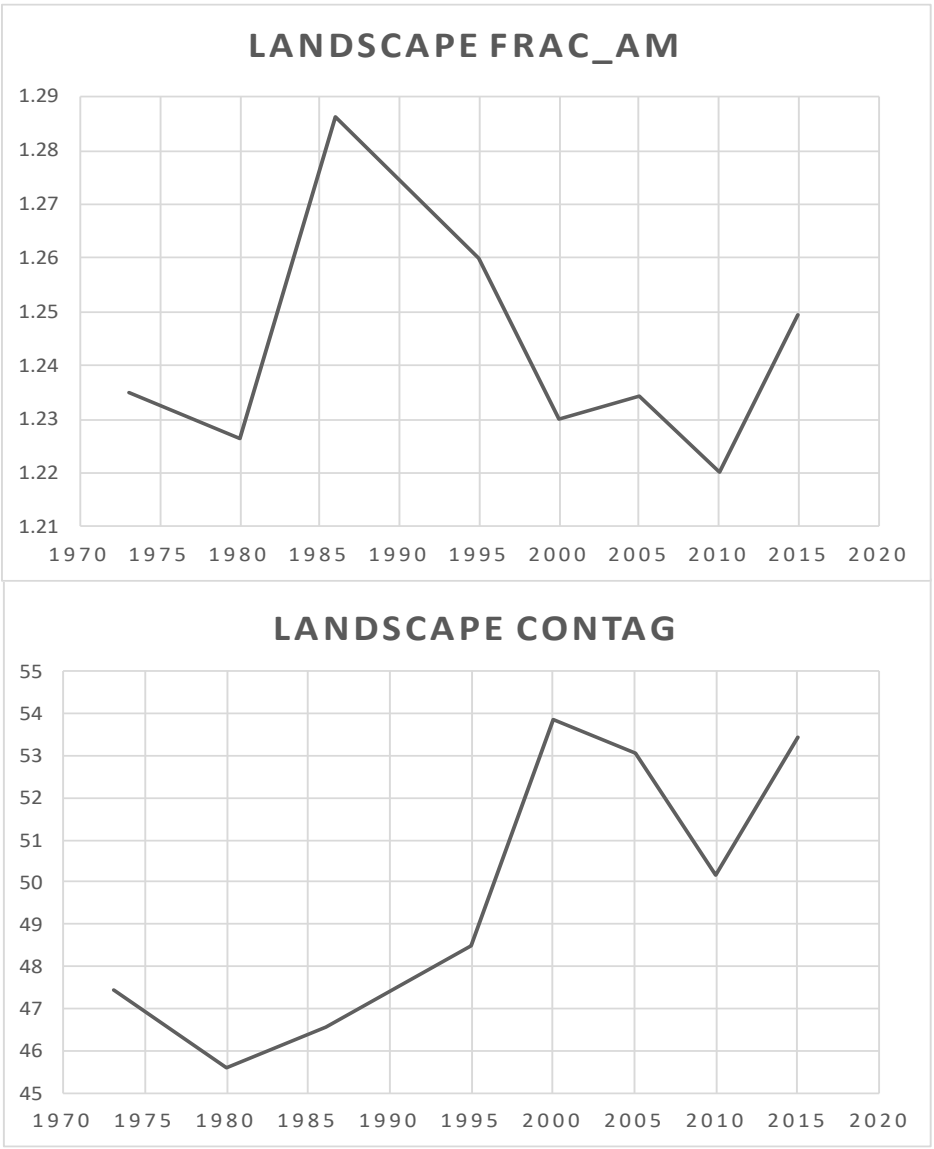

Figure 4.1 Landscape metrics of the study area

Figure (a) FRAC_AM is the Area Weighted Mean Fractal Index; (b) CONTAG is the Contiguity Index (%)

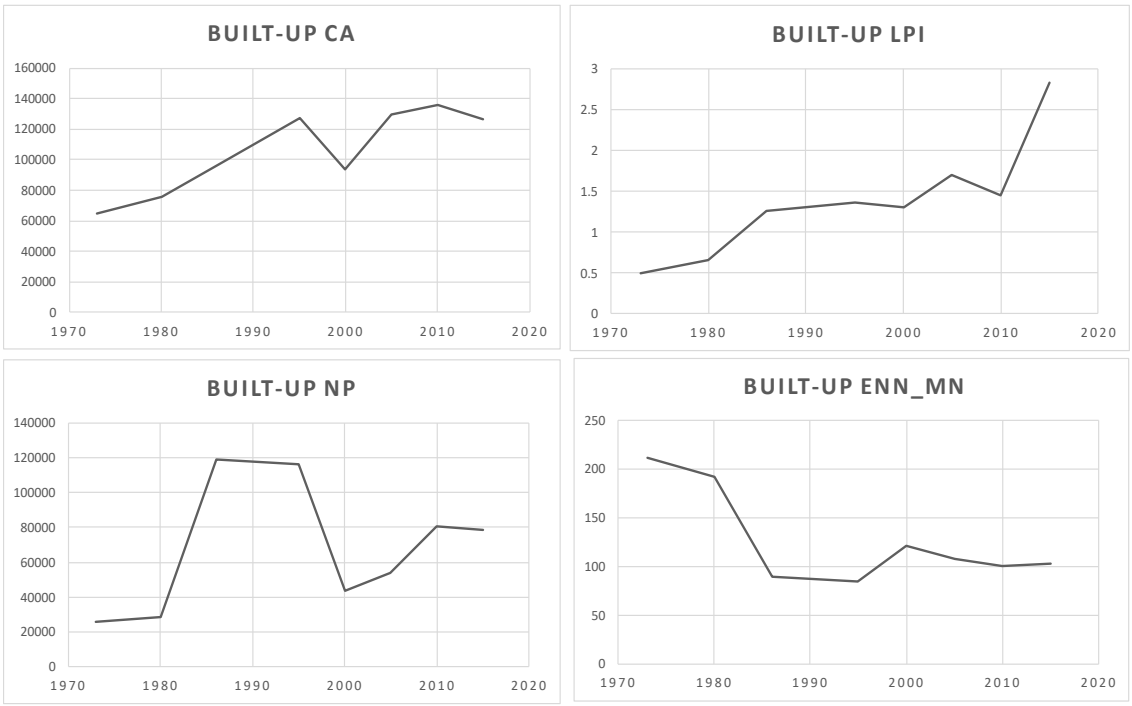

Figure 4.2 Urban/Built-Up land cover class metrics of the study area

CA is the Class Area of built-up land cover in hectares; (b) PA is the number of patches; (c) LPI is the Largest Patch Index (%); (d) ENN_MN is the Euclidian Mean Nearest Neighbor Distance

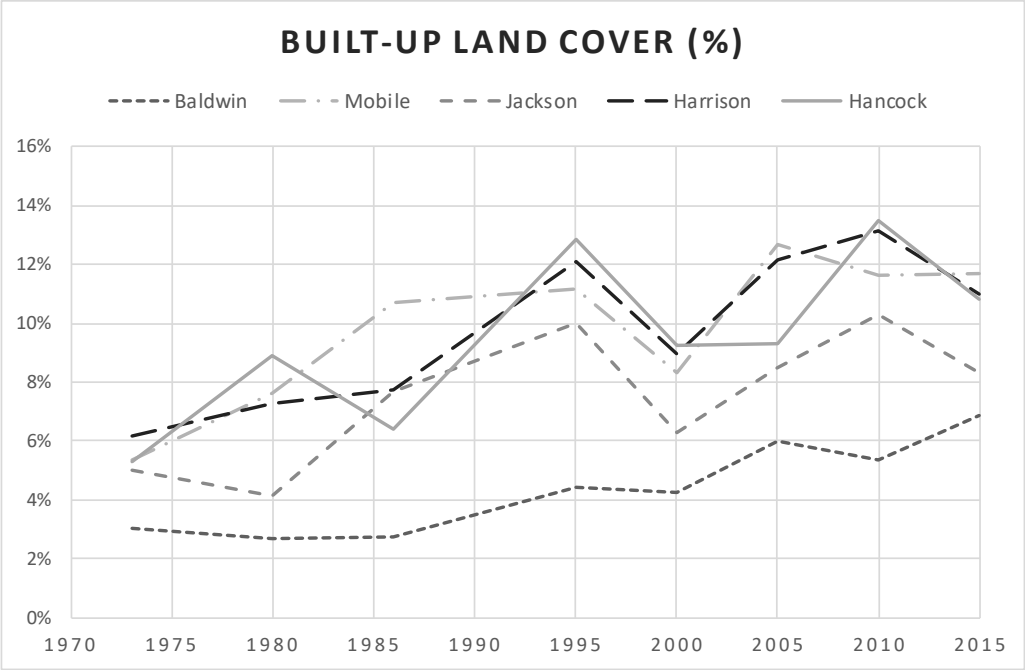

Figure 4.3 Built-up/Urban class Percent Land Cover (PLAND) for each County

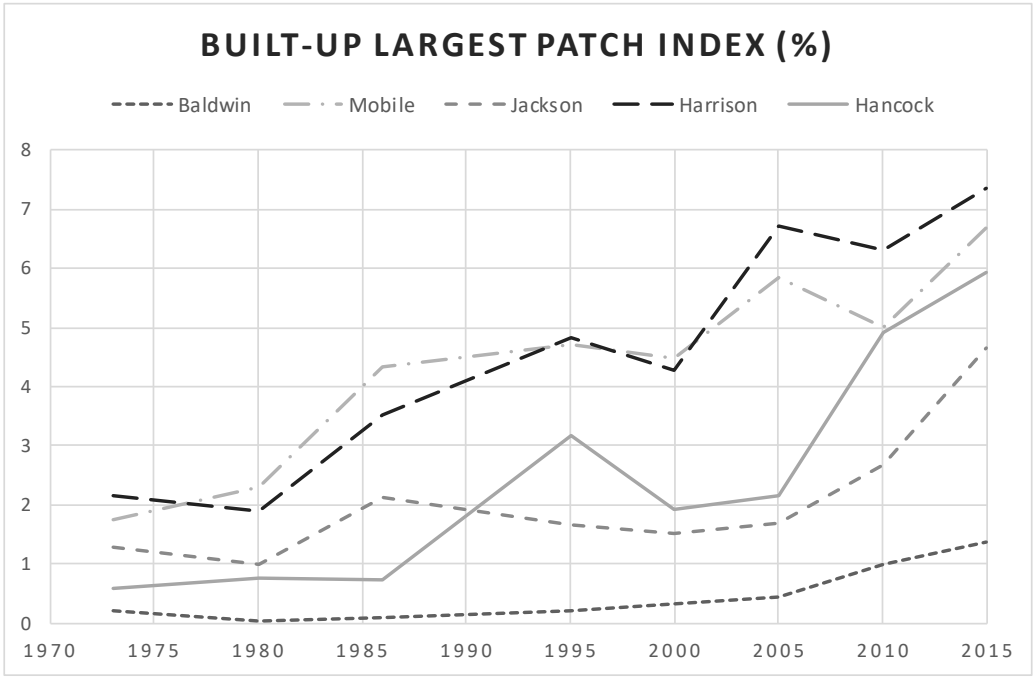

Figure 4.4 Built-up/Urban class Largest Patch Index (LPI) for each County

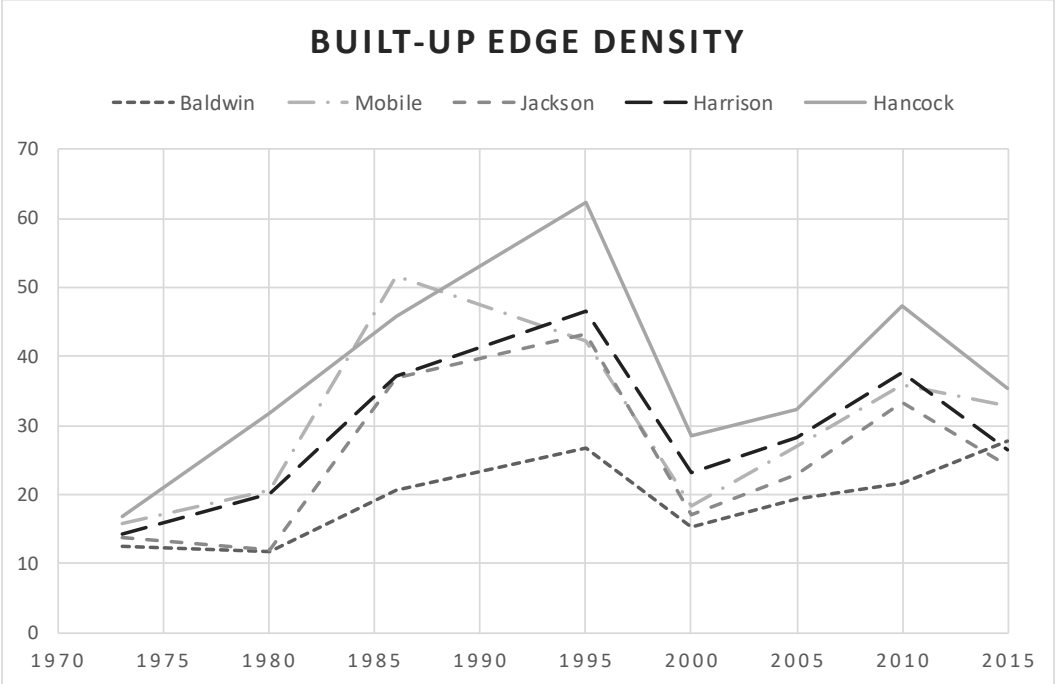

Figure 4.5 Built-up Edge Density (ED) for each County

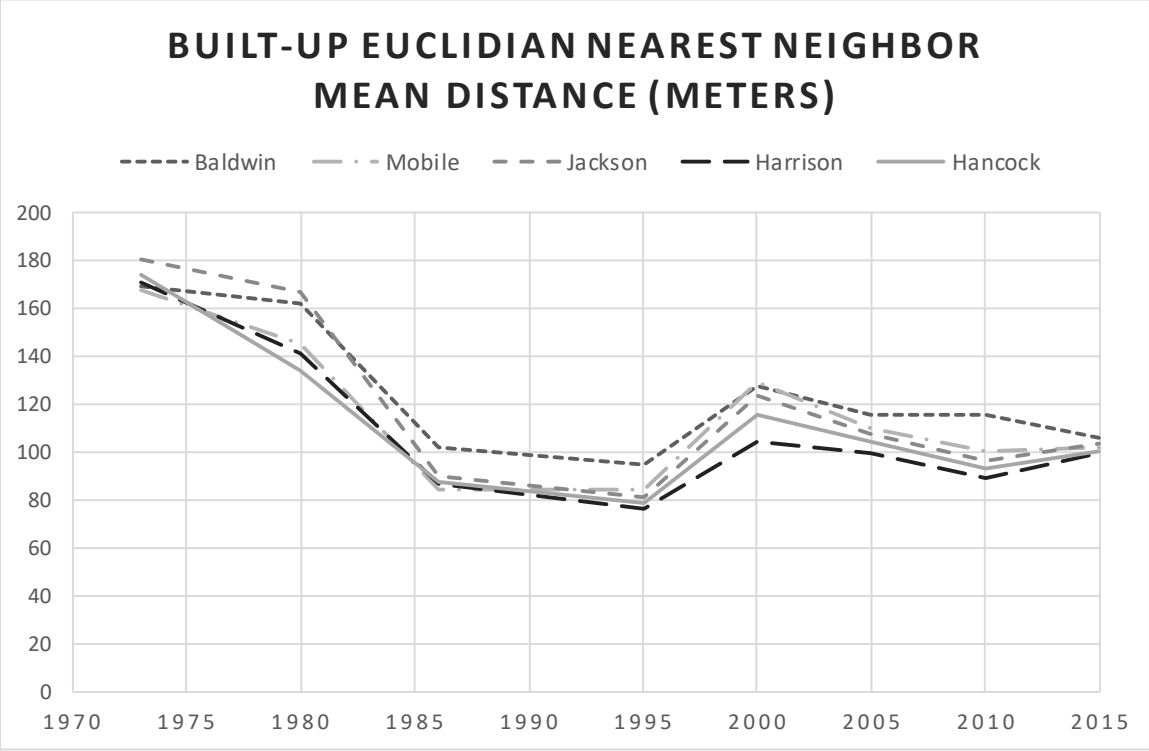

Figure 4.6 Built-up Euclidian Nearest Neighbor Mean Distance (ENN_MN)

Table 4.10 Proportion of land cover types (PLAND) of the study area

	1973 (%)	1980 (%)	1986 (%)	1995 (%)	2000 (%)	2005 (%)	2010 (%)	2015 (%)
Urban/Built-up	4.8571	5.7505	7.3071	9.6021	7.0998	9.8163	10.2406	9.6014
Agriculture	7.6592	8.5444	8.786	6.9021	7.4011	4.9565	8.1961	5.3229
Forest	36.845	34.5475	37.357	41.6563	42.9364	41.1794	39.2242	44.1301
Rangeland	17.491	16.808	10.9735	6.5061	9.157	10.3275	9.1427	8.2288
Marshes	3.7275	4.6395	5.2606	4.8843	2.9908	3.2483	2.8453	2.626
Barren	0.5123	0.7471	0.6304	1.5498	0.9895	0.6992	0.8649	0.6599
Water	28.908	28.9631	29.6855	28.8992	29.4254	29.7729	29.4862	29.431

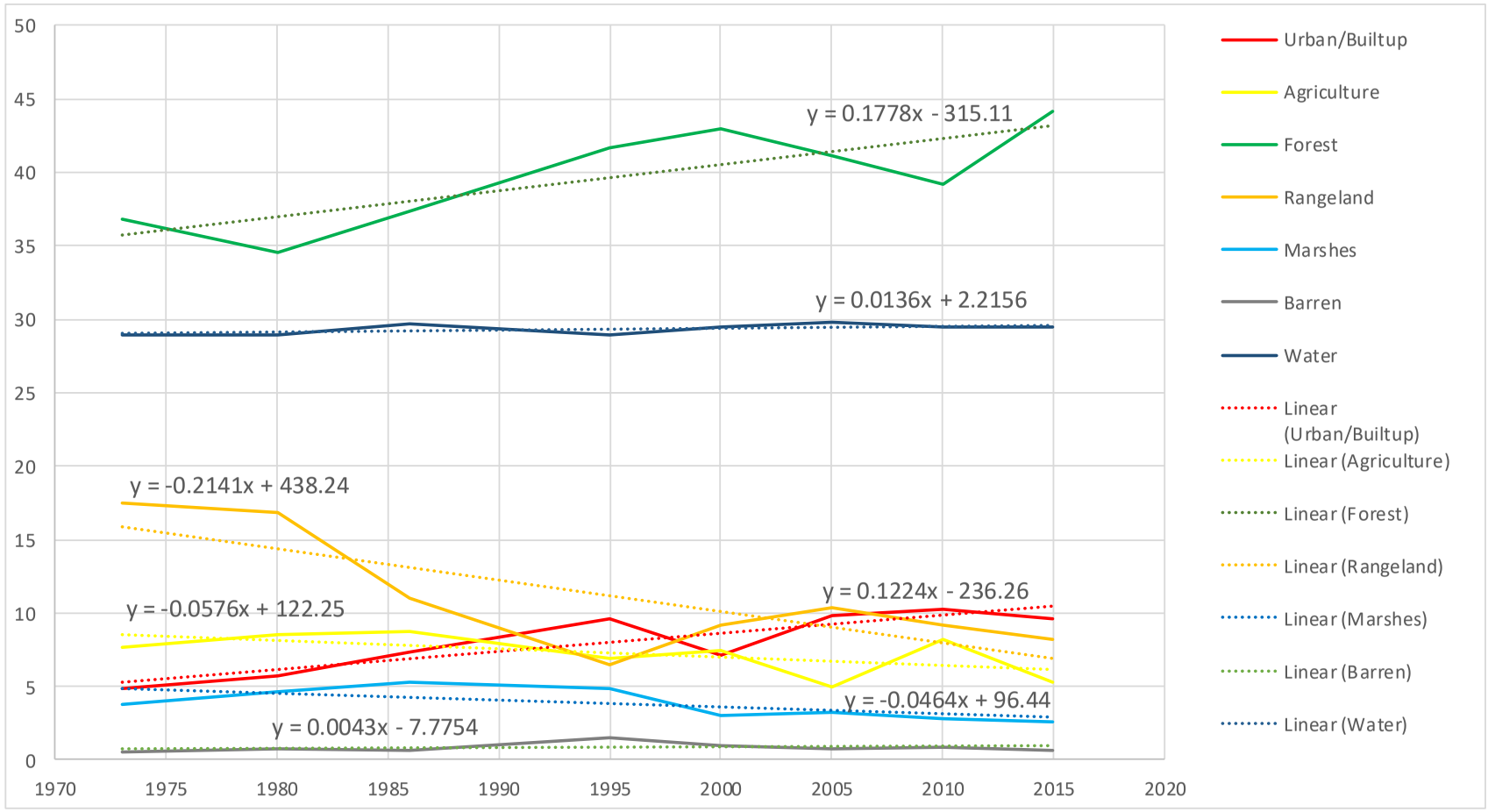

Figure 4.7 The proportion of land cover types in the whole study area (PLAND)

4.6 Classified Time Series

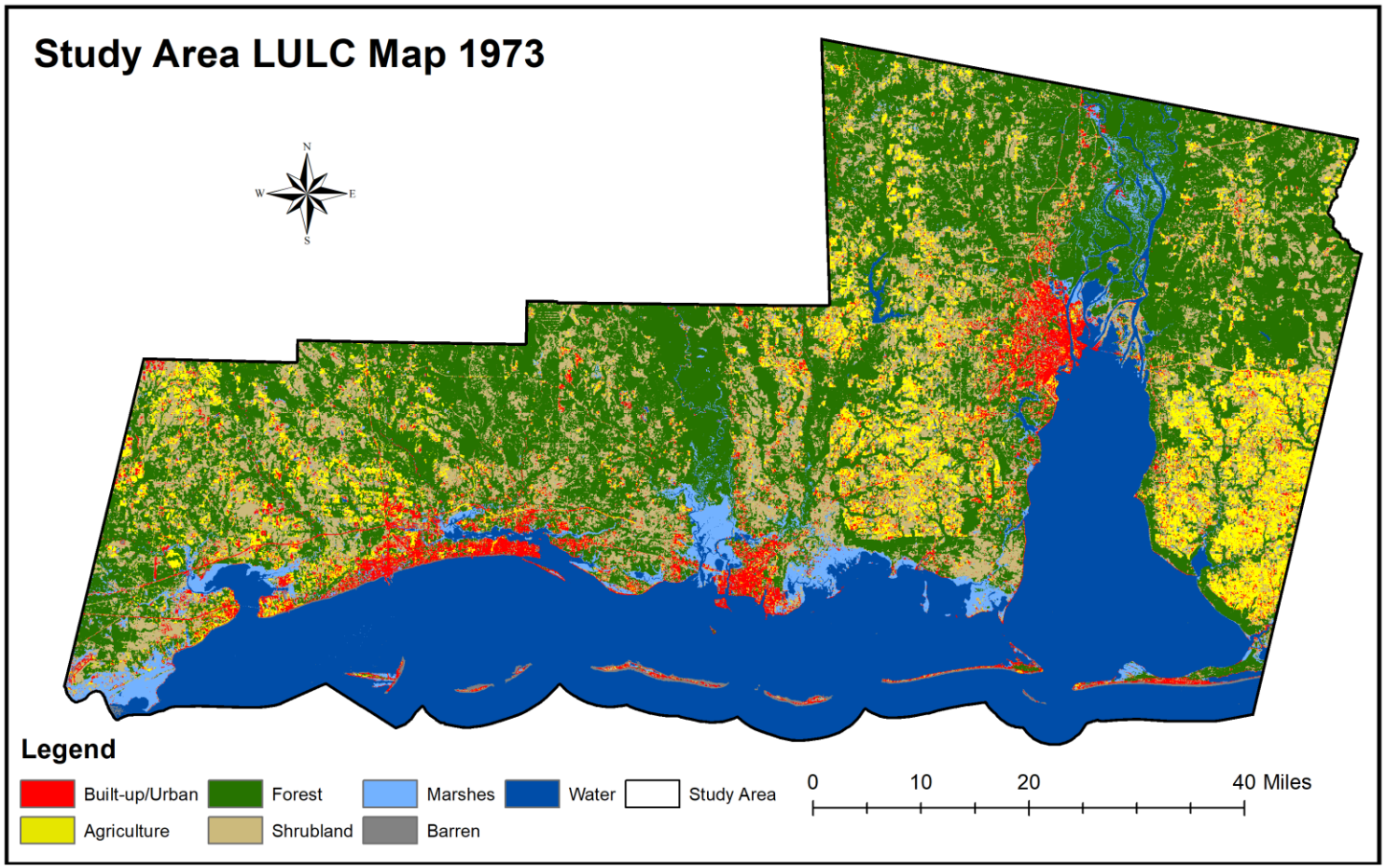

Figure 4.8 1973 LULC map of the study area

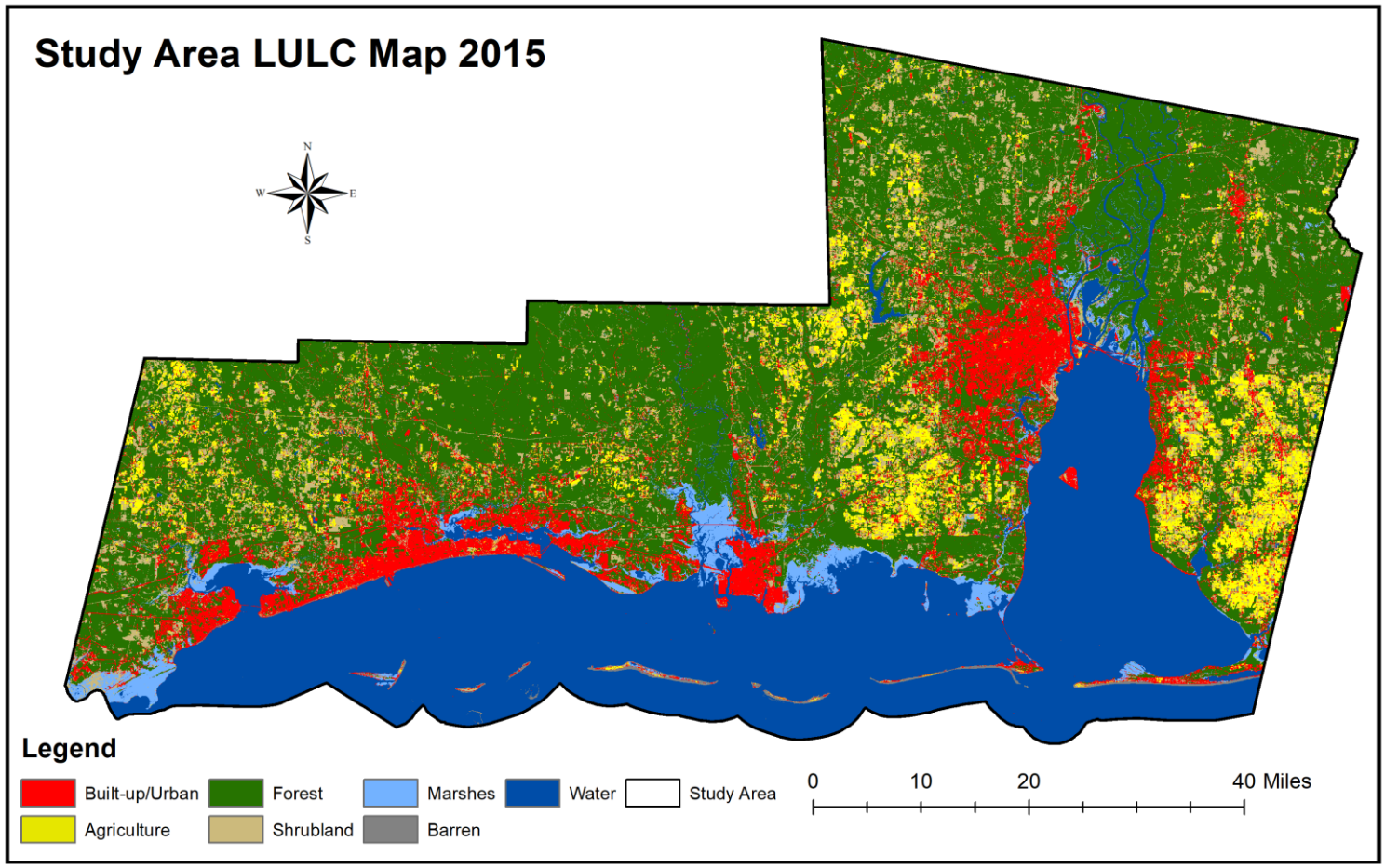

Figure 4.9 2015 LULC map of the study area

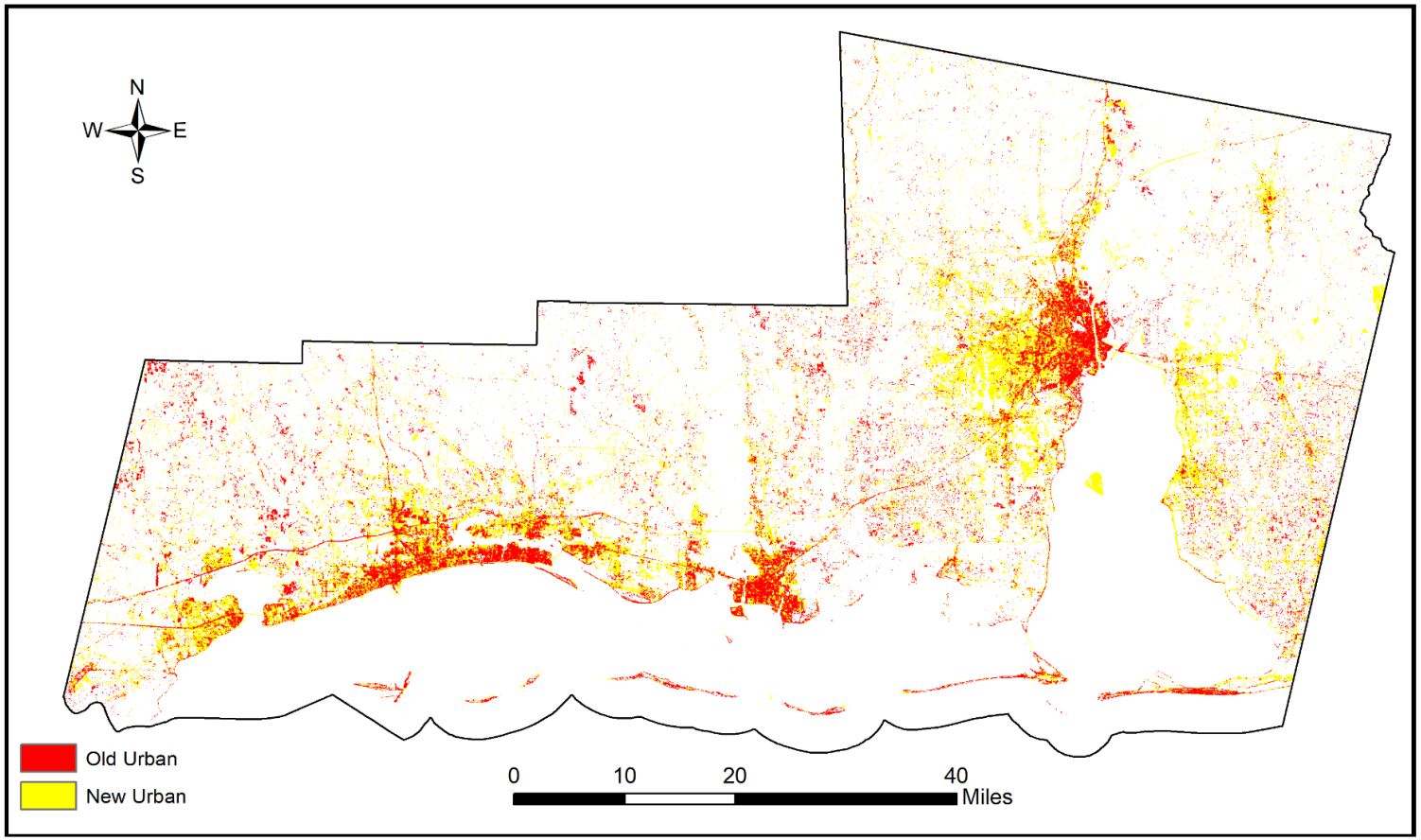

Figure 4.10 Changes in urban land cover between 1973 and 2015

"Old Urban" references the 1973 urban land cover and "New Urban" refers to 2015 land cover

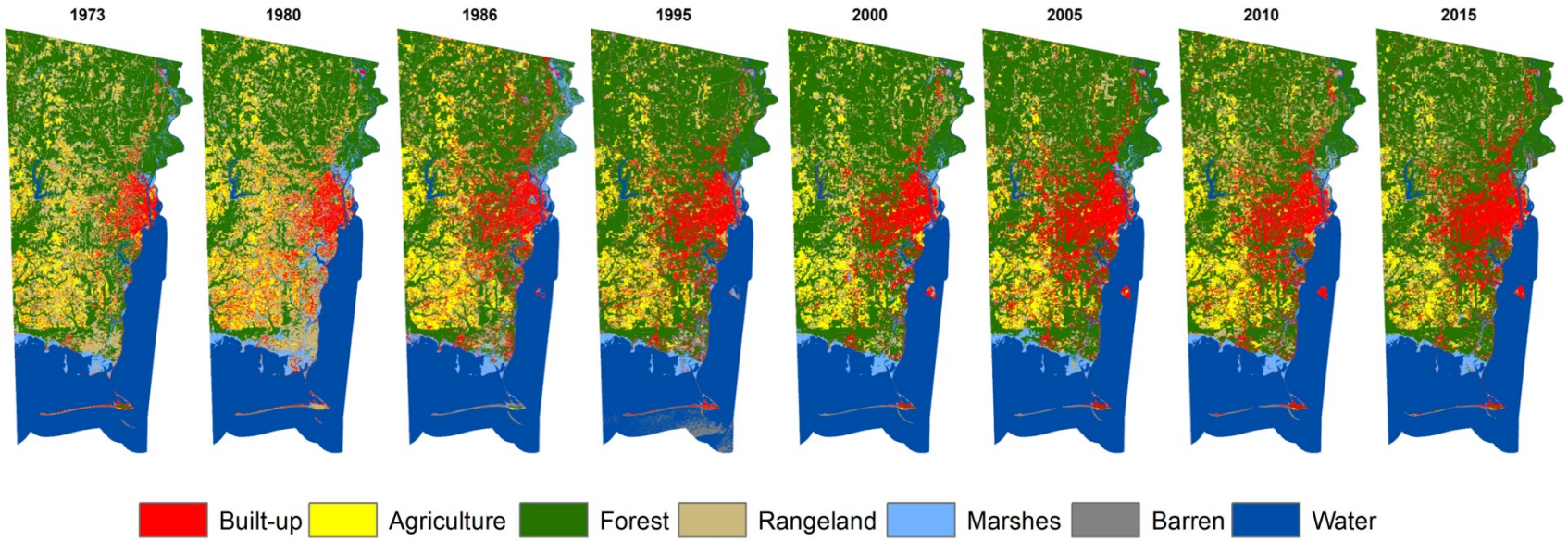

Figure 4.11 LULC maps of Mobile County, Alabama from 1973 to 2015

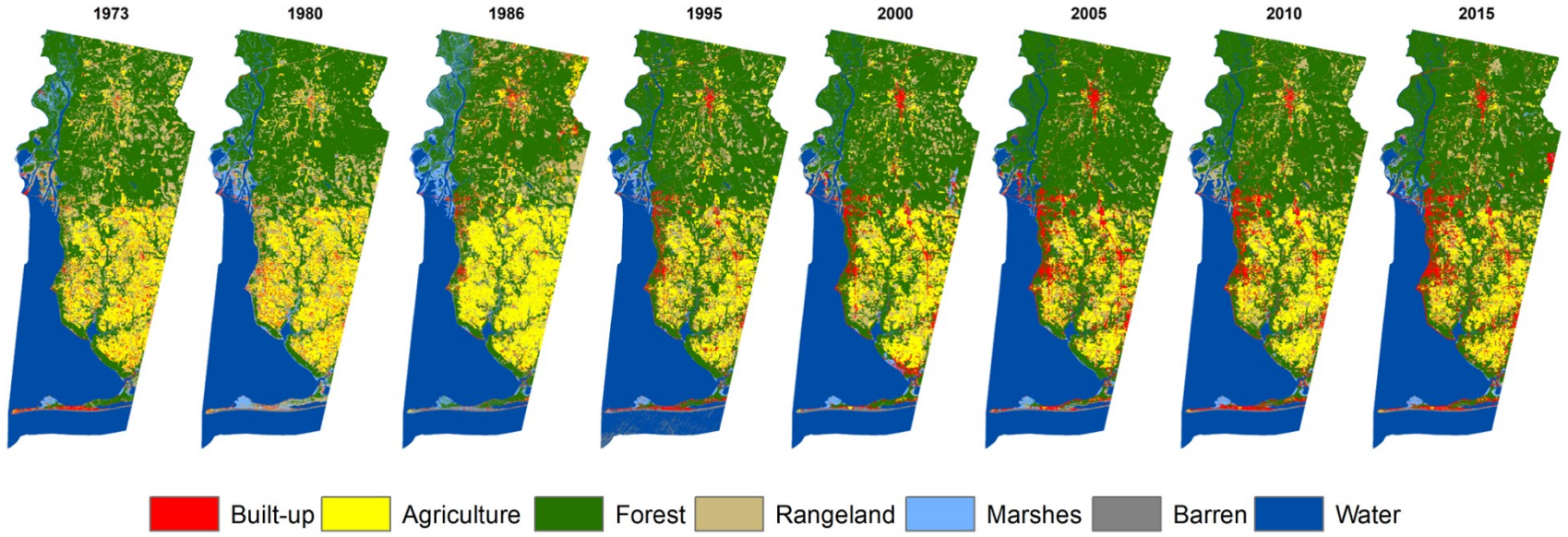

Figure 4.12 LULC maps of Baldwin County, Alabama from 1973 to 2015

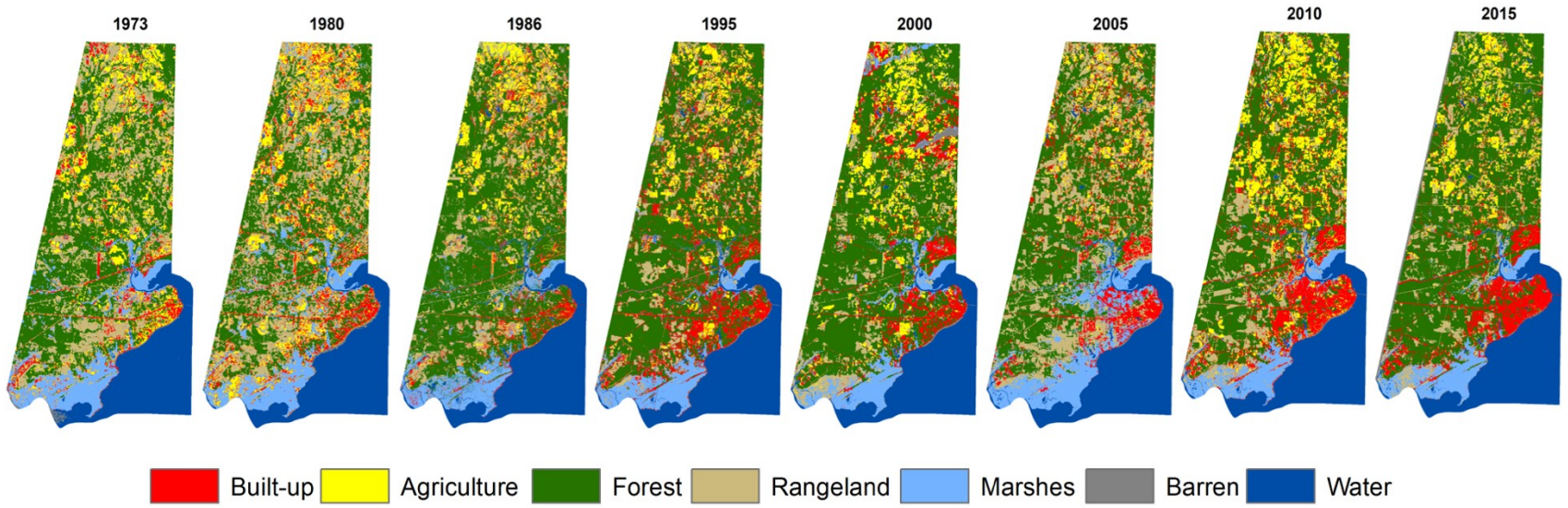

Figure 4.13 LULC maps of Hancock County, Mississippi from 1973 to 2015

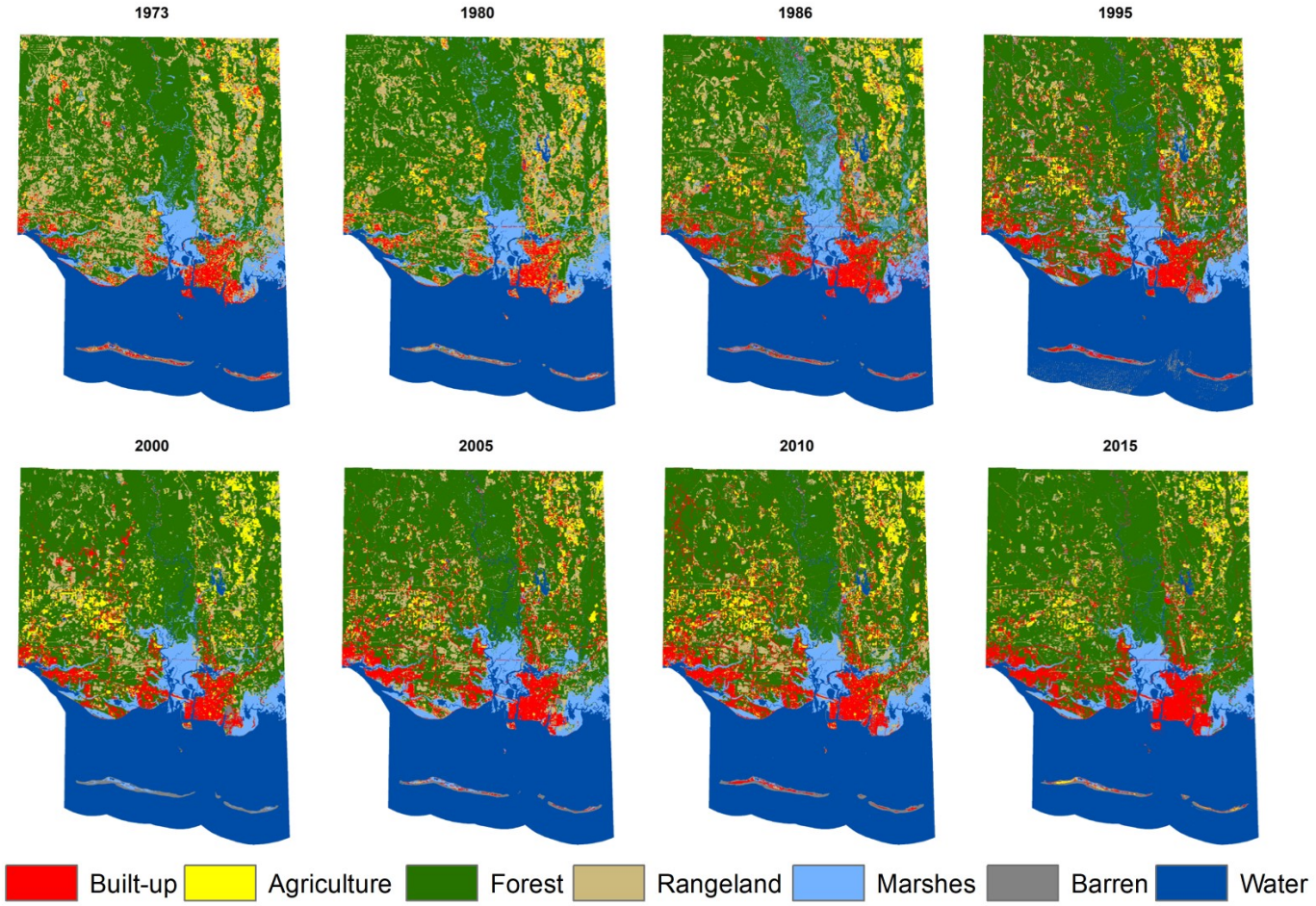

Figure 4.14 LULC maps of Jackson County, Mississippi from 1973 to 2015

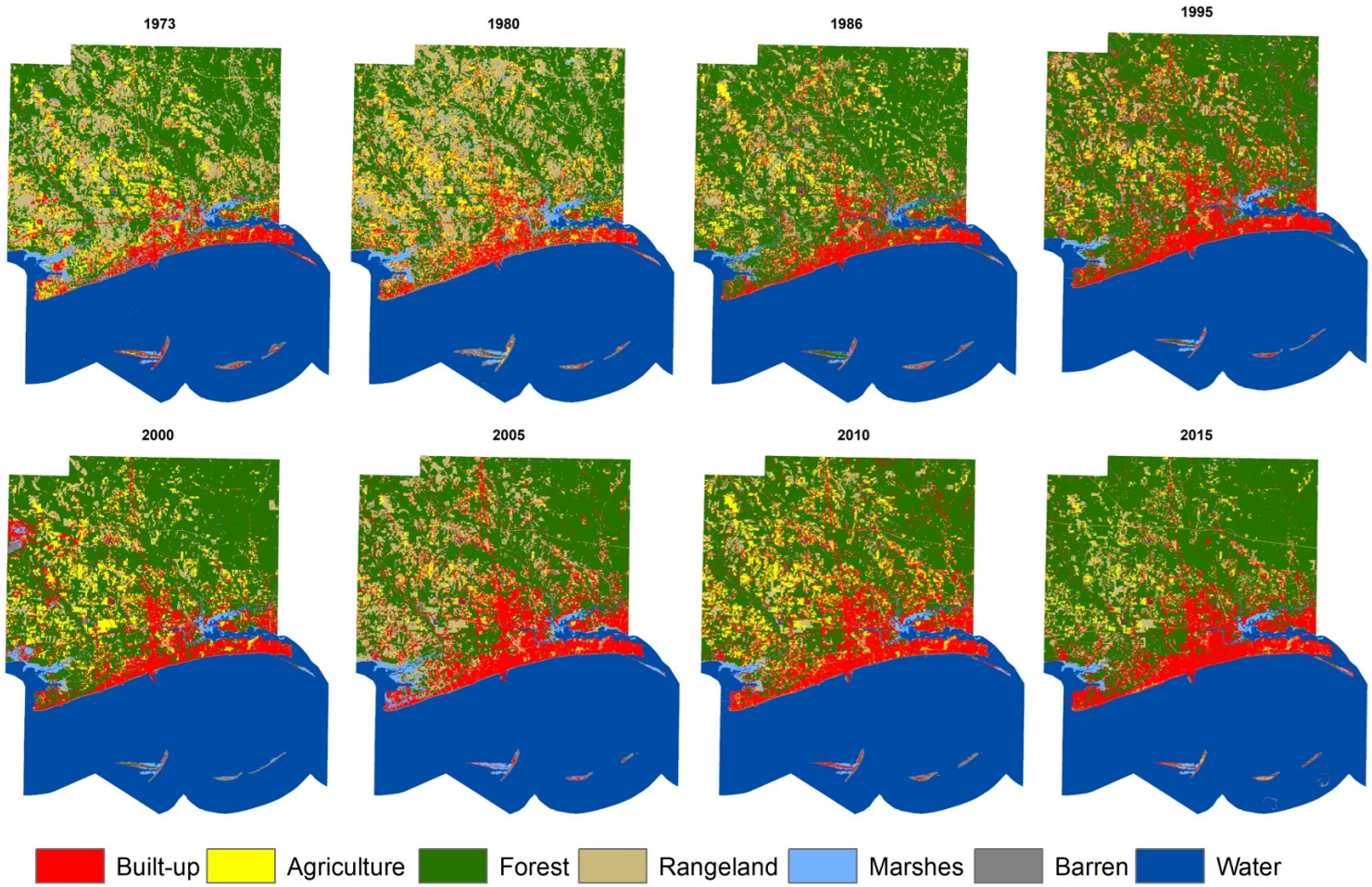

Figure 4.15 LULC maps of Harrison County, Mississippi from 1973 to 2015

CHAPTER V

CONCLUSION

5.1 Conclusion

In this study, we demonstrated the use of landscape metrics to describe the thematic urban land cover change and enhance the information derived from a classic LULC study. There was an overall increase in the urban land cover with the highest rate occurring in the early years from 1973 to 1990, followed by decreasing rate in the following years (1990-2015). During the earlier years (1973-1986), the study area experienced high levels of fragmentation due to urban sprawl, and in later period (1990-2015) fragmentation decreased. The urban land cover became more aggregate, which can be attributed to the "fill-in" effect. The Alabama counties, Mobile and Baldwin, experienced the highest rate of urban development per year in contrast with the Mississippi Counties. The increase of urban land cover mostly affected the Rangeland and Agriculture land covers, with Rangeland having a high negative and statistically significant correlation to the increase in urban land cover. The use of landscape metrics in conjunction with classic LULC study allows for a better understanding of the land cover change assessment. The outcome of this study can be incorporated in coastal development planning and serve as the primary evaluation of the Gulf Coast environment to help reduce degradation for this environmentally sensitive region.

5.2 Limitations

Although great care was taken during the signature collection process for the supervised classification, the calculated accuracy of the classified maps was lower than expected. This accuracy problem made the change detection less capable causing misrepresentation in several scenes. For some of the scenes (1973 and 1980), there were few or no high-resolution aerial imagery to verify training sites accurately, and some newer images were used to do most of the accuracy point collection in conjunction with the actual scenes. The disparity in spatial resolution of the MSS scenes (60 m) and the non-MSS scenes (30 m) may also have contributed to lowering the change detection accuracy, especially for the urban classification type. There was some difficulty in interrupting some of the second level landscape metrics, which is a known problem in research dealing with landscape metrics and applying them to describe the development of urban land cover (Bhatta et al., 2010; Ji et al., 2006). Describing urban development can be more difficult due to the complexity of factors that result in land cover change, and especially in the Gulf Coast, a growing region with a variety of economic, social and political factors. Similarly, this region is affected by a variety of natural disasters of which may have different effects on the land cover types that are outside the scope of this study.

Although the classification accuracy of this study met the standard for Anderson level I LULC classification requirements, better classification methods can be used to achieve high classification accuracy, such as using sub-pixel classification methods, and object-based classification. Using the data derived from this study, a refocus on a smaller scale to a city level or metropolitan level can give more insight into the urban

development of major cities within this region. Further statistical analysis of the landscape metrics can yield more insight into the distributions of other land covers that are in this study.

REFERENCES

Anderson, J.R., Hardy, E.E., Roach, J.T., Witmer, R.E., 1976. A Land Use and Land Cover Classification System for Use with Remote Sensor Data. USGS Prof. Pap. 964 28.

Anthony, A., Atwood, J., August, P. V., Byron, C., Cobb, S., Foster, C., Fry, C., Gold, A., Hagos, K., Heffner, L., others, 2009. Coastal lagoons and climate change: ecological and social ramifications in the US Atlantic and Gulf coast ecosystems 14.

Arvidson, T., Goward, S.N., Gasch, J., Williams, D., 2006. Landsat-7 long-term acquisition plan: Development and validation. Photogramm. Eng. Remote Sensing 72, 1137–1146. doi:10.14358/pers.72.10.1137

Bailey, R.G., Avers, P.E., King, T., McNab, W.H., 1994. 1994, Ecoregions and subregions of the United States with supplementary table of map unit descriptions: Washington, DC. US Dep. Agric. For. Serv. scale 1.

Bhatta, B., Saraswati, S., Bandyopadhyay, D., 2010. Urban sprawl measurement from remote sensing data. Appl. Geogr. 30, 731–740. doi:10.1016/j.apgeog.2010.02.002

Campbell, J.B., Wynne, R.H., 2011. Introduction to remote sensing. Guilford Press.

Chang, K., 2006. Geographic information system. Wiley Online Library.

Chavez, P.S.J., 1989. Radiometric calibration of Landsat thematic mapper multispectral images. Photogramm. Eng. Remote Sensing 55, 1285–1294.

Colwell, R.N., 1966. Uses and limitations of multispectral remote sensing.

Congalton, R.G., 1991. A review of assessing the accuracy of classifications of remotely sensed data. Remote Sens. Environ. 37, 35–46. doi:10.1016/0034-4257(91)90048-B

Coppin, P., Jonckheere, I., Nackaerts, K., Muys, B., Lambin, E., 2004. Review

ArticleDigital change detection methods in ecosystem monitoring: a review. Int. J. Remote Sens. 25, 1565–1596. doi:10.1080/0143116031000101675

Creel, L., 2003. Ripple effects: Population and coastal regions. Popul. Ref. Bur. 8.

Crossett, K., Culliton, T., Wiley, P., Goodspeed, T., 2004. Population Trends Along the Coastal United States : 1980-2008. Coast. Trends Ser. Rep. 1980–2008.

D. Lu, Weng, Q., 2007. A survey of image classification methods and techniques for improving classification performance International Journal of Remote Sensing. Int. J. Remote Sens. 8, 823–870. doi:10.1080/01431160600746456

Davis, S.M., Swain, P.H., 1978. Remote sensing: the quantitative approach. New York, McGraw-Hill Int. B. Co., 1978. 405 p.

Dolan, A.H., Walker, I.J., 2006. Understanding vulnerability of coastal communities to climate change related risks. J. Coast. Res. SI 39, 1316–1323.

Duckham, M., Goodchild, M.F., Worboys, M., 2004. Foundations of geographic information science. CRC Press.

Ellis, J.T., Spruce, J.P., Swann, R.A., Smoot, J.C., Hilbert, K.W., 2011. An assessment of coastal land-use and land-cover change from 1974-2008 in the vicinity of Mobile Bay, Alabama. J. Coast. Conserv. 15, 139–149. doi:10.1007/s11852-010-0127-y

Ennis, B., Peterson, M.S., Strange, T.P., 2014. Modeling of Inundation Characteristics of a Microtidal Saltmarsh, Grand Bay National Estuarine Research Reserve, Mississippi. J. Coast. Res. 295, 635–646. doi:10.2112/JCOASTRES-D-13-00041.1

Fitzpatrick-Lins, K., 1981. Comparison of sampling procedures and data analysis for a land-use and land-cover map. Photogramm. Eng. Remote Sensing 47, 343–351.

Foody, G.M., Mathur, A., 2004. A relative evaluation of multiclass image classification

by support vector machines. IEEE Trans. Geosci. Remote Sens. 42, 1335–1343. doi:10.1109/TGRS.2004.827257

Gutman, G., Janetos, A.C., Justice, C.O., Moran, E.F., Mustard, J.F., Rindfuss, R.R., Skole, D., Turner II, B.L., Cochrane, M. a, 2004. Land Change Science: Observing, Monitoring, and Understanding Trajectories of Change on the Earth's Surface, Remote Sensing and Digital Image Processing. doi:10.1007/978-1-4020-2562-4_7

Ha, I., 2007. Recreational demand for a gulf coast tourism destination. J. Econ. Econ. Educ. Res. 8, 51.

Hepner, G.F., Logan, T., Pitter, N., Bryant, N., 1989. Artificial Neural Network Classification Using a Minimal Training Set : Comparison to Conventional Supervised Classification. Photogramm. Eng. Remote Sensing 56, 469–473.

Herold, M., Scepan, J., Clarke, K.C., 2002. The use of remote sensing and landscape metrics to describe structures and changes in urban land uses. Environ. Plan. A 34, 1443–1458. doi:10.1068/a3496

Homer, C., Dewitz, J., Fry, J., Coan, M., Hossain, N., Larson, C., Herold, N., Mckerrow, A., Vandriel, J.N., Wickham, J., 2007. Completion of the 2001 National Land Cover Database for the Conterminous United States. Photogramm. Eng. Remote Sens. 73, 337–341. doi:citeulike-article-id:4035881

Homer, C., Huang, C., Yang, L., Wylie, B., Coan, M., 2004. Development of a 2001 national land-cover database for the United States. Photogramm. Eng. Remote Sens. 70, 829–840.

Hudson, W.D., Ramm, C.W., 1987. Correct formulation of the kappa-coefficient of agreement. Photogramm. Eng. Remote Sensing 53, 421.

IPCC, 2007. The Physical Science Basis: Working Group I Contribution to the Fourth Assessment Report of the IPCC, Climate Change 2007. Cambridge University Press. doi:volume

Jensen, J., 2005. Introductory Digital Image Analysis. A Remote Sensing Perspective. Prentice Hall, Inc.,Old Tappan, NJ, Columbus, NC.

Jensen, J., Cowen, D., 1999. Remote sensing of urban suburban infrastructure and socio-economic attributes. Photogramm. Eng. Remote Sensing 65, 611–622.

Jensen, J.R., 1986. Introductory digital image processing: a remote sensing perspective. Univ. of South Carolina, Columbus.

Ji, W., Ma, J., Twibell, R.W., Underhill, K., 2006. Characterizing urban sprawl using multi-stage remote sensing images and landscape metrics. Comput. Environ. Urban Syst. 30, 861–879. doi:10.1016/j.compenvurbsys.2005.09.002

Kolios, S., Stylios, C.D., 2013. Identification of land cover/land use changes in the greater area of the Preveza peninsula in Greece using Landsat satellite data. Appl. Geogr. 40, 150–160. doi:10.1016/j.apgeog.2013.02.005

F.A. Kruse, A.B. Lefkoff, J.W. Boardman, K.B. Heidebrecht, A.T. Shapiro, P.J. Barloon, A.F.H.G., 1993. The Spectral Image Processing System (SIPS) - Interactive Visualization and Analysis of Imaging Spectrometer Data. Remote Sens. Environ. https://doi.org/10.1016/0034-4257(93)90013-N

Lauer, D.T., Morain, S. a, Salomonson, V. V, 1997. The Landsat Program : Its Origins, Evolution, and Impacts. Photogramm. Eng. Remote Sens. 63, 831–838.

Lhermitte, S., Verbesselt, J., Jonckheere, I., Nackaerts, K., van Aardt, J.A.N., Verstraeten, W.W., Coppin, P., 2008. Hierarchical image segmentation based on

similarity of NDVI time series. Remote Sens. Environ. 112, 506–521. doi:10.1016/j.rse.2007.05.018

Li, T., Meng, Q., 2016. Forest dynamics to precipitation and temperature in the Gulf of Mexico coastal region. Int. J. Biometeorol. doi:10.1007/s00484-016-1266-0

Li, X., Gong, P., Liang, L., 2015. A 30-year (1984–2013) record of annual urban dynamics of Beijing City derived from Landsat data. Remote Sens. Environ. 166, 78–90. doi:10.1016/j.rse.2015.06.007

Lipp, E.K., Farrah, S.A., Rose, J.B., 2001. Assessment and Impact Of Microbial Fecal Pollution And Human Enteric Pathogens In A Coastal Community. Mar. Pollut. Bull. 42, 286–293.

Lu, D., Tian, H., Zhou, G., Ge, H., 2008. Regional mapping of human settlements in southeastern China with multisensor remotely sensed data. Remote Sens. Environ. 112, 3668–3679. doi:10.1016/j.rse.2008.05.009

Macleod, R.D., Congalton, R.G., 1998. Quantitative comparison of change-detection algorithms for monitoring eelgrass from remotely sensed data. Photogramm. Eng. Remote Sensing 64, 207–216.

Malila, W.A., 1980. Change vector analysis: An approach for detecting forest changes with Landsat. LARS Symp. 326–335.

McGarial, K., Marks, B., 1995. FRAGSTAT: Spatial pattern analysis program for quantifying landscape structure. United States Dep. Agric. Pacific Northwest Res. Station. 120 pages. doi:10.1061/(ASCE)0733-9437(2005)131:1(94) CE

Mcgarigal, K., 2001. Landscape metrics for categorical map aatterns 2001, 1–77. doi:10.1007/BF00162741

Megahed, Y., Cabral, P., Silva, J., Caetano, M., 2015. Land Cover Mapping Analysis and Urban Growth Modelling Using Remote Sensing Techniques in Greater Cairo Region—Egypt. ISPRS Int. J. Geo-Information 4, 1750–1769. doi:10.3390/ijgi4031750

Nemmour, H., Chibani, Y., 2006. Multiple support vector machines for land cover change detection: An application for mapping urban extensions. ISPRS J. Photogramm. Remote Sens. 61, 125–133. doi:10.1016/j.isprsjprs.2006.09.004

NRCS, U., 2008. Geospatial data gateway.

O'Hara, C.G., King, J.S., Cartwright, J.H., King, R.L., 2003. Multitemporal land use and land cover classification of urbanized areas within sensitive coastal environments. IEEE Trans. Geosci. Remote Sens. 41, 2005–2014. doi:10.1109/TGRS.2003.816573

Oivanki, S.M., 1998. Geology and geomorphology of the Mississippi Gulf Coast. Mar. Resour. Hist. Mississippi Gulf Coast 2, 291–308.

Otukei, J.R., Blaschke, T., 2010. Land cover change assessment using decision trees, support vector machines and maximum likelihood classification algorithms. Int. J. Appl. Earth Obs. Geoinf. 12. https://doi.org/10.1016/j.jag.2009.11.002.

Paola, J.D., Schowengerdt, R.A., 1995. A review and analysis of backpropagation neural networks for classification of remotely-sensed multi-spectral imagery. Int. J. Remote Sens. 16, 3033–3058. doi:10.1080/01431169508954607

Petterson, J.S., Stanley, L.D., Glazier, E., Philipp, J., 2006. A Preliminary Assessment of Social and Economic Impacts Associated with Hurricane A Preliminary Assessment of Social Impacts Associated with Hurricane Katrina. Source Am. Anthropol. New Ser. 108, 643–670.

Riebsame, W.E., Meyer, W.B., Turner, B.L., 1994. Modeling land use and cover as part of global environmental change. Clim. Change 28, 45–64. doi:10.1007/BF01094100

Rogan, J., Chen, D., 2004. Remote sensing technology for mapping and monitoring land-cover and land-use change. Prog. Plann. 61, 301–325. doi:10.1007/s10708-004-4936-0

Rosenfield, G.H., Fitzpatrick-Lins, K., 1986. A coefficient of agreement as a measure of thematic classification accuracy. Photogramm. Eng. Remote Sens. 52, 223–227.

Roy, D.P., Wulder, M.A., Loveland, T.R., C.E., W., Allen, R.G., Anderson, M.C., Helder, D., Irons, J.R., Johnson, D.M., Kennedy, R., Scambos, T.A., Schaaf, C.B., Schott, J.R., Sheng, Y., Vermote, E.F., Belward, A.S., Bindschadler, R., Cohen, W.B., Gao, F., Hipple, J.D., Hostert, P., Huntington, J., Justice, C.O., Kilic, A., Kovalskyy, V., Lee, Z.P., Lymburner, L., Masek, J.G., McCorkel, J., Shuai, Y., Trezza, R., Vogelmann, J., Wynne, R.H., Zhu, Z., 2014. Landsat-8: Science and product vision for terrestrial global change research. Remote Sens. Environ. 145, 154–172. doi:10.1016/j.rse.2014.02.001

Rozenstein, O., Karnieli, A., 2011. Comparison of methods for land-use classification incorporating remote sensing and GIS inputs. Appl. Geogr. 31, 533–544. doi:10.1016/j.apgeog.2010.11.006

Samek, J.H., Xuan Lan, D., Silapathong, C., Navanagruha, C., Masturah Syed Abdullah, S., Gunawan, I., Crisostomo, B., Hilario, F., Hoang, M.H., Skole, D.L., Chomentowski, W., Salas, W.A., Sanjaya, H., 2012. Land use and land cover change in Southeast Asia, 6th ed, Land Change Science: Observing, Monitoring and Understanding Trajectories of Change on the Earth's Surface. Springer Science \&

Business Media. doi:10.1007/978-1-4020-2562-4

Singh, A., 2017. Review Article Digital change detection techniques using remotely-sensed data 1161. doi:10.1080/01431168908903939

Storey, J., Scaramuzza, P., Schmidt, G., Barsi, J., 2005. Landsat 7 Scan Line Corrector-Off Gap-Filled Product Gap-Filled Product Development Process. Proc. Pecora 16, 23–27.

Tipsword, H.L., Setzer, F.M., Smith, F.L.J., 1966. Interpretation of Depositional Environment in Gulf Coast Petroleum Exploration from Paleoecology and Related Stratigraphy. Am. Assoc. Pet. Geol. 16, 119–130.

Tuia, D., Persello, C., Bruzzone, L., 2016. Domain adaptation for the classification of remote sensing data: An overview of recent advances. IEEE Geosci. Remote Sens. Mag. 4, 41–57. doi:10.1109/MGRS.2016.2548504

Turner, B.L.I., Lambin, E., Reenberg, A., 2008. Land Change Science Special Feature: The emergence of land change science for global environmental change and sustainability. PNAS 105, 20666–20671. doi:10.1073/pnas.0704119104

Turner, M.G., Ruscher, C.L., 1988. Changes in landscape patterns in Georgia, USA. Landsc. Ecol. 1, 241–251. doi:10.1007/BF00157696

Twilley, R.R., Barron, E.J., Gholz, H.L., Harwell, M.A., Miller, R.L., Reed, D.J., Rose, J.B., Siemann, E.H., Wetzel, R.G., Zimmerman, R.J., 2001. Confronting climate change in the Gulf Coast region: prospects for sustaining our ecological heritage.

U.S. Census Bureau, 2011. Selected housing charactersitcs, 2007-2011 American Community Survey 5-year estimates [WWW Document]. URL http://factfinder2.census.gov/faces/tableservices/jsf/pages/productview.xhtml?pid=A

CS_11_5YR_DP04

Urban, D.L., Shugart, H.H., 1987. Landscape ecology: a hierarchical perspective can help scientists understand spatial patterns. Bioscience 37.

USGS, 2017a. EarthExplorer [WWW Document]. U.S. Dep. Inter. U.S. Geol. Surv. URL https://earthexplorer.usgs.gov/

USGS, 2017b. Product Guide: Landsat 4-7 Surface Reflectance (LEDAPS) Product. USGS Prof. Pap. 8, 38.

Weng, Q., 2012. Remote sensing of impervious surfaces in the urban areas: Requirements, methods, and trends. Remote Sens. Environ. 117, 34–49. doi:10.1016/j.rse.2011.02.030

Weng, Q., 2002. Land use change analysis in the Zhujiang Delta of China using satellite remote sensing, GIS and stochastic modelling. J. Environ. Manage. 64, 273–284. doi:10.1006/jema.2001.0509

Williamson, M., 1997. THE IMPACT OF SPACE TECHNOLOGY ON SOCIETY. IEEE Int. Symp. Technol. Soc. 139–147. doi:10.1109/ISTAS.1997.658873

Wulder, M.A., Masek, J.G., Cohen, W.B., Loveland, T.R., Woodcock, C.E., 2012. Opening the archive: How free data has enabled the science and monitoring promise of Landsat. Remote Sens. Environ. 122, 2–10. doi:10.1016/j.rse.2012.01.010

Yu, X., Zhang, A., Hou, X., Li, M., Xia, Y., 2012. Multi-temporal remote sensing of land cover change and urban sprawl in the coastal city of Yantai, China. Int. J. Digit. Earth 6, 1–18. doi:10.1080/17538947.2011.653995

Zhang, Y., Guindon, B., Cihlar, J., 2002. An image transform to characterize and compensate for spatial variations in thin cloud contamination of Landsat images.

Remote Sens. Environ. 82, 173–187. doi:10.1016/S0034-4257(02)00034-2

Zhang, Y., Li, S., Guo, Z., 2015. The Evolution of the Coastal Economy: The Role of Working Waterfronts in the Alabama Gulf Coast. Sustainability 7, 4310–4322. doi:10.3390/su7044310